Climate Dynamics
https://doi.org/10.1007/s00382-019-04630-6

Dynamical downscaling the impact of spring Western US land surface temperature on the 2015 flood extremes at the Southern Great Plains: effect of domain choice, dynamic cores and land surface parameterization

Ismaila Diallo[1] · Yongkang Xue[1,2] · Qian Li[3] · Fernando De Sales[4] · Wei Li[5]

Received: 6 June 2018 / Accepted: 10 January 2019
© Springer-Verlag GmbH Germany, part of Springer Nature 2019

Abstract

Recent studies have shown that spring land surface temperature (LST) and subsurface temperature (SUBT) over the high elevation areas in the western US (WUS) have significant impacts on the downstream summer droughts/floods in North America. In this paper, both the National Centers for Environmental Prediction—Global Forecast System (NCEP-GFS) general circulation model (GCM) and the weather research and forecasting (WRF) regional climate model (RCM) are employed, where RCM scenarios utilized initial and lateral boundary conditions derived from the corresponding NCEP-GFS scenarios. Here we use a late spring flood in the US Southern Great Plains (SGP) case to examine whether simulation of the LST/SUBT downstream effects is sensitive to the domain size choice, change in dynamical cores within the same model, as well as to the representation of surface processes parameterizations. Although all RCM experiments with different settings simulate reasonably geographical patterns of observed LST and precipitation anomalies, we found that the choice of the domain size is crucial for proper downscaling the LST/SUBT downstream effects to accurately produce the observed precipitation/LST anomalies over the SGP/WUS, respectively, along with the associated large-scale features. The southern boundary location has been identified to be crucial in producing the SGP Low Level Jet strength, which in turn brings more moisture from the Gulf of Mexico to the SGP and thereby resulting in a better simulation of the precipitation anomaly in that area. The sensitivity of the simulation of the LST/SUBT downstream effect to dynamical cores is assessed by inter-comparing the Non-hydrostatic Mesoscale Model (NMM) and the Advanced Research WRF dynamic cores. We find NMM was better at generating the large-scale eastward wave train, a crucial process associated with the LST/SUBT downstream effect. Meanwhile, this study also shows that the LST/SUBT downstream effects were not significantly dependent on the surface process parameterizations, although the Simplified Simple Biosphere model version 3 (SSiB3) highlighted a better performance over SSiB2.

Keywords Dynamical downscaling · US flood · Land surface temperature and subsurface temperature · Southern Great Plains · Dynamical cores · Regional climate model

Electronic supplementary material The online version of this article (https://doi.org/10.1007/s00382-019-04630-6) contains supplementary material, which is available to authorized users.

✉ Ismaila Diallo
idiallo@ucla.edu

[1] Department of Geography, University of California Los Angeles (UCLA), 315 Portola Plaza, 1255 Bunche Hall, Los Angeles, CA 90095-1524, USA

[2] Department of Atmospheric and Oceanic Sciences, UCLA, Los Angeles, CA 90095-1524, USA

[3] Institute of Atmospheric Physics, Chinese Academy of Sciences, Beijing 100029, China

[4] Department of Geography, San Diego State University, San Diego, CA, USA

[5] IMSG and Environmental Modeling Center/National Center for Environmental Prediction (NCEP), NOAA, College Park, MD 20740, USA

Published online: 21 January 2019

1 Introduction

Extreme late spring/summer climate anomalies, including droughts, floods, and heat waves in the United States (US), have been investigated by many studies and are attracting interest due to severe drought/flood conditions in the last decade (Dong et al. 2011; Mei and Wang 2012; Hoerling et al. 2014; Xue et al. 2012, 2016, 2018, Pu et al. 2016; Saini et al. 2016; and many others). For instance, during May 2015, Southern Great Plains and several adjacent cities (hereafter referred to as SGP) saw one of their wettest Mays on record, which was neither fully predicted nor anticipated. This flood event made headlines in many media outlets, while the property damage in Houston alone was estimated to more than $40 million (Wang et al. 2015; Mekonnen et al. 2016; Xue et al. 2018). Despite considerable progress in understanding processes controlling the US seasonal/intra-seasonal rainfall variability (see review by Koster et al. 2017, and paper cited therein), accurately predicting these extreme events in models still remains a challenge (Xue et al. 2018). Using observational datasets, Xue et al. (2012, 2016, 2018) have shown a significant relationship between the spring land surface temperature (LST) anomaly over the Western US (WUS) and the late spring/summer precipitation anomaly over the SGP. Meanwhile, their modeling studies show that a spring warm (cold) LST anomaly over the WUS is associated with the development of late spring/summer flooding (drought) over the SGP. Nowadays, it has been established that the spring subsurface soil temperature (SUBT) and LST anomalies over the WUS play important roles in controlling the hydroclimatic regime variability over the SGP. Using an atmospheric Global Climate Model (GCM) and a Regional Climate Model (RCM), Xue et al. (2016) have investigated the potential contribution of the spring WUS LST/SUBT anomalies to the unprecedented 2011 summer SGP drought and have found that the 2011 cool WUS LST/SUBT anomalies were able to simulate about 30% and 34% of the observed 2011 SGP subsequent drought and abnormal heat, respectively. Likewise, Xue et al. (2018) suggested that the warm WUS spring LST/SUBT anomaly increased the likelihood of development of the unprecedented May 2015 SGP flooding.

Despite providing useful information, coarse resolutions GCMs have limitations in properly representing the LST/SUBT downstream precipitation anomalies (Xue et al. 2012, 2016, 2018). Further, GCMs have difficulties to accurately capture the detailed processes associated with regional and/or local climate variability and changes (Giorgi and Mearns 1999; Rummukainen 2010; Xue et al. 2014; Mariotti et al. 2014; Diallo et al. 2015, 2016; Fotso-Nguemo et al. 2017; among others). RCMs have been developed to regionally enhance the GCM information, and they can yield fine scale climate information often different from that derived from GCMs due to their ability to capture regional processes and forcing (e.g. land use, coastlines, topography, valley wind… etc.) (Xue et al. 2007; De Sales and Xue 2011; Diallo et al. 2012, 2014; Torma et al. 2015; Poan et al. 2018; and many others). In fact, RCMs have been useful for different purposes and they have also been shown to be able to dependably replicate the spatial and temporal distributions of mean climate along with its associated large scale circulations for specific regions (see reviews by Xue et al. 2014, and references therein). However, several uncertainties arise when setting RCM nesting experiments. Such uncertainties include, sensitivity to the domain size choice and boundary location (Seth and Giorgi 1998; Vannitsem and Chomé 2005; Xue et al. 2007; Leduc and Laprise 2009; Gao et al. 2012; Bhaskaran et al. 2012; Browne and Sylla 2012; Centella-Artola et al. 2015; Dash et al. 2015; Song et al. 2018), dynamical core within the same RCM (Gallus and Bresch 2006; Dodla et al. 2011; Litta et al. 2012), and land surface process parameterizations (e.g. Xue et al. 2001, 2010; Vidale et al. 2003; Chen et al. 2014; Li et al. 2016). For instance, focusing on the Contiguous United States (CONUS) summer climate, Xue et al. (2007) found that when utilizing initial and lateral boundary conditions (LBCs) derived from Reanalysis II, the southern boundary location in the Gulf of Mexico (GoM) and Caribbean Sea is most relevant, while Bhaskaran et al. (2012), using the HadRM3P, found that better simulation of the Indian summer monsoon precipitation variability was only achieved when considering a smaller domain. Centella-Artola et al. (2015) used the PRECIS RCM to assess the effect of domain size over the Caribbean region. They found that key rainfall characteristics, such us the Caribbean Low Level Jet and the mid-summer drought are insensitive to domain size. A study by Browne and Sylla (2012) pointed out that over West Africa, a large domain extending to the Atlantic Ocean is required to capture the monsoon processes and to generate the mesoscale convective cells (e.g. African Easterly Waves and squall lines). On the other hand, Van Den Broeke et al. (2017) carried out a study to investigate the sensitivity of the central United States warm season to various land surface schemes (LSMs) coupled to the weather research and forecasting (WRF) model version 3.6 (WRF3.6; Skamarock et al. 2008). Their study found that the sign/magnitude of the simulated central United States precipitation and temperature biases are sensitive to the LSMs, though they all appear suitable for investigating the effect of land use land cover changes over the region. Xue et al. (2001) inter-compared the Eta model coupled with the Simplified Simple Biosphere biophysical model (SSiB; Xue et al. 1991; Zhan et al. 2003) and the Eta model coupled with the Bucket model and concluded that the land parameterizations are crucial in reproducing the 1993 US flooding.

Early LST/SUBT modeling efforts (Xue et al. 2012, 2016, 2018) have: (1) confirmed the observed relationship between the WUS LST anomalies and the development of SGP drought/floods, and (2) proposed the mechanism through which the WUS LST/SUBT anomaly contributes to the development and strengthening of droughts/floods over the SGP. Given that the LST anomaly affects the downstream precipitation anomaly through perturbation of large-scale circulation, Xue et al. (2012) demonstrated that to study the LST/SUBT downstream effect the RCM LBCs for particular scenarios should be obtained from the GCM with the corresponding scenarios and therefore might inherit some biases from their boundary conditions. While much of these early works have been devoted to the reproduction of the observed relationship with emphasis on the mechanism of LST/SUBT downstream effects in North America, it has been demonstrated that proper RCM downscaling plays an important role in identifying this effect. Additional research focusing mainly on investigating the uncertainties with the RCM dynamical downscaling method (DDM) of the LST/SUBT downstream effects in a comprehensive way is therefore warranted and the present study aims to address this subject. In this study using the WRF modeling system (Skamarock et al. 2008; Janjic et al. 2001) coupled to different versions of the SSiB vegetation biophysical process model as land surface models, we extend the works of Xue et al. (2012, 2016, 2018) and undertake a more detailed analysis using the 2015 late spring flood in the US SGP case to investigate uncertainties associated with the RCM DDM of the LST/SUBT downstream effects. Our study has three goals: (1) explore how the domain size choice and boundary locations could affect the DDM of the LST/SUBT downstream effect, (2) investigate to what extent change in dynamical core within the same RCM could affect the DDM of the LST/SUBT downstream effects along with its associated large-scale mechanism, and (3) examine the sensitivity of the simulation of the LST/SUBT downstream effect to different land surface parameterizations.

The paper is organized as follows. Section 2 describes the model configurations and different experimental designs as well as the methodology adopted and the reference datasets used for validation and comparisons. Results and discussions are presented in Sect. 3, where the impact of domain size choice and boundary position, and the impact of change of dynamical core within the same RCM are examined, before providing an overview of the impact of land surface parameterization on the DDM of the LST/SUBT downstream effects. Finally, the important results obtained in this study are given in the summary and concluding Sect. 4.

2 Models description, experimental design and method

2.1 Models description

The experiments for this study were performed using the WRF modeling system (WRF) (Skamarock et al. 2008; Janjic et al. 2001) and the National Centers for Environmental Prediction - Global Forecast System (NCEP-GFS, Kanamitsu et al. 2002).

2.1.1 The weather research and forecasting (WRF) modeling system

The WRF is a multi-agency modeling system with flexible resolution and parameterization, which is applicable for both numerical weather prediction and regional climate modeling. The WRF model is a state-of-the-art mesoscale model framework with two available dynamic cores: (1) the Non-hydrostatic Mesoscale Model (NMM) developed by the National Oceanic and Atmospheric Administration—National Centers for Environmental Prediction (NOAA-NCEP) (Janjic et al. 2001), and (2) the Advanced Research WRF (ARW) developed by the National Center for Atmospheric Research (NCAR) (Skamarock et al. 2008). The NMM core is a fully regional, compressible, non-hydrostatic mesoscale model, and primitive-equation that uses a terrain-following hybrid sigma-pressure vertical coordinate together with the Arakawa E-grid staggering for horizontal discretization. The ARW core is a fully compressible, Eulerian non-hydrostatic model, using a terrain-following hydrostatic-pressure vertical coordinate, together with vertical grid stretching and Arakawa C–grid staggering for the horizontal grid. Various versions of the SSiB vegetation biophysical process land surface model (LSMs) have been implemented into the WRF modeling system. There are 13 vegetation-cover types in SSiB LSM map. These include crop land, mixed broadleaf and needleleaf tree, grassland, tropical forest, shrubs, etc, as listed in the work by Xue et al. (2001). The NMM core has been coupled to both the second version of SSiB (SSiB2) and the third version of SSiB (SSiB3). These atmosphere-land surface coupled models will hereafter be referred to as NMM/SSiB2 and NMM/SSiB3, respectively. The state-of-the-art vegetation biophysical model, SSiB2, preserves at the atmosphere-land surface interface water, energy, and momentum conservation, while estimating the photosynthesis processes for surface carbon emission and transpiration (Xue et al. 1991, 2003; Sun et al. 1998; Zhan et al. 2003). The physics in the SSiB2 and the SSiB3 biophysical LSM are identical except for the snow scheme, which has

an important impact on the spring LST simulation. In fact, SSiB3 employs a multi-layer coupled surface snow hydrology and radiative transfer schemes, while SSiB2 utilizes a one-layer snow hydrology model. For further detailed description of SSiB3 and/or SSiB2 along with their main differences, readers are referred to Sun and Xue (2001), Xue et al. (2003), and Oaida et al. (2015). For the ARW dynamical core, SSiB3 is utilized to describe the land surface bio-geophysical processes (hereafter referred to as ARW/SSiB3). Table 1 summarizes the selected physics and parameterizations of NMM/SSiB3, and ARW/SSiB3, as well as NMM/SSiB2 selected to complete an array of numerical experiments which are outlined in Sect. 2.2.

2.1.2 NCEP global forecast system (GFS)

The NCEP-GFS simulations provide initial and LBCs for the WRF integrations. The NCEP-GFS is utilized in this study as an atmospheric global climate model with a T62 horizontal resolution grid and 17 vertical levels. T62 corresponds to 94 latitudes unequally spaced and 192 longitudes equally spaced grid points, with a horizontal resolution of roughly 1.91° by 1.875° latitude/longitude grids at the equator. The selected NCEP-GFS physics and parameterizations include: (1) a non-local scheme for the boundary layer vertical diffusion (Hong and Pan 1996), (2) a modified Simplified Arakawa-Schubert (SAS) for cumulus convection (Hong and Pan 1998), (3) the cloud microphysics of Zhao and Carr (1997) updated by Moorthi et al. (2001) to determine the prognostic cloud water and ice mixing ratios, and (4) an upgraded solar radiation transfer scheme of Hou et al. (2002). For the representation of land surface processes, the second version of the SSiB (SSiB2) was implemented into the NCEP-GFS. The global atmosphere-land surface coupled model will hereafter be referenced as GFS/SSiB2.

2.2 Experimental design

To isolate the potential contribution of the warm early spring LST/SUBT anomalies over the WUS to the extreme wet anomaly conditions in May 2015 over the SGP, we conducted two sets of scenarios simulations using GFS/SSiB2 under the same initial atmospheric and land surface conditions, sea surface temperature (SST), and sea-ice forcing. The 2015 atmospheric and land surface conditions from the NCEP analysis as well as the NCEP 2015 global real time SST analysis and observed sea ice were utilized for the boundary conditions of GFS/SSiB2 in all scenarios cases. In the first scenario case, we imposed the specified warm LST and SUBT anomalies over the WUS based on the observed 2 m-temperature difference between March 2015 and the March mean value for 1981–2015 with tuning (supplemental Figure S1) and aimed to reproduce the observed 2 m-temperature anomaly over WUS. Since there is no long-period large-scale SUBT measurement, we generated the SUBT anomaly based on the 2 m-temperature from Climate Anomaly Monitoring System observation (CAMS, Fan and Van den Dool 2008). The warm anomalies are only imposed at the first step of the model integration, after which the model updated both LST and SUBT based on its free integration. This scenario serves as control case and is referred to as "GFS/SSiB2 Case SUBT". In the second GFS/SSiB2 scenario case, hereafter referred to as "GFS/SSiB2 Case noSUBT", no warm initial LST and SUBT anomalies were imposed, while all other settings, including physics parameterizations and initial conditions, remained similar to GFS/SSiB2 Case SUBT. Since ensemble runs are usually needed to reduce uncertainties associated with initial conditions, and to derive a robust result, we completed each scenario case with a seven-member ensemble of continuous simulations. The ensemble members were initialized at 00z, 27, 28,

Table 1 Selected physical set-up of NMM/SSiB3, ARW/SSiB3, and NMM/SSiB2

	NMM/SSiB3	ARW/SSiB3	NMM/SSiB2
Dynamical core	NMM	ARW	NMM
Land-surface model (LSM)	SSiB3	SSiB3	SSiB2
Planetary boundary layer (PBL)	Mellor–Yamada–Janjic (MYJ; Janjic 2001)	Yonsei University (Hong et al. 2006)	MYJ (Janjic 2001)
Cumulus convection	Betts–Miller–Janjic (BMJ; Janjic 2001)	Grell and Devenyi (2002)	BMJ (Janjic 2001)
Cloud microphysics	Ferrier (Ferrier 1994)	Ferrier (Ferrier 1994)	Ferrier (Ferrier 1994)
Shortwave	NOAA GFDL (Fels and Schwarzkopf 1981)	Fu–Liou–Gu (Gu et al. 2011)	NOAA GFDL (Fels and Schwarzkopf 1981)
Longwave	NOAA GFDL (Fels and Schwarzkopf 1981)	Fu–Liou–Gu (Gu et al. 2011)	NOAA GFDL (Fels and Schwarzkopf 1981)
Horizontal grid-spacing	50 km (0.44° × 0.44°)	50 km (0.44° × 0.44°)	50 km (0.44° × 0.44°)
Initial and lateral boundary conditions (LBCs)	GFS/SSiB2 Case 2015 GSF/SSiB2 Case noSUBT	GFS/SSiB2 Case 2015 GSF/SSiB2 Case noSUBT	GFS/SSiB2 Case 2015 GSF/SSiB2 Case noSUBT

29, 30, 31 March 2015, 01, 02 April 2015 and ended at 00z 01 June 2015. There was no re-initialization of any fields for the different integrations. Both GFS/SSiB2 scenario cases are identical with the results from Xue et al. (2018).

In order to investigate the sensitivity of the domain size choice, along with the location of the boundary on the teleconnections between the remote warm large-scale early spring LST and SUBT anomalies over the WUS and the development of the May 2015 extreme precipitation over the SGP, while large-scale driving fields from NCEP-GFS are kept identical, we carried out each NMM/SSiB3 scenario cases using three different domains encompassing most of central North America and the adjoining Pacific and Atlantic oceans (Fig. 1). The NMM/SSiB3 was used for this set of experiments. Each experiment was set-up on a horizontal grid-spacing of 0.44° x 0.44° latitude/longitude (about 50×50 km) with 38 vertical levels grid extending from the surface to 50 hPa. The first domain [Domain 1 (D1)] is a very large domain, encompassing the continental United States, almost all of Canada, Mexico, and a substantial portion of the adjoining Atlantic and Pacific oceans. The second domain [Domain 2 (D2)], with a westward (eastward) shift of the eastern (western) boundary location, was the domain previously used in Xue et al. (2016). In the third domain [Domain 3 (D3)], the southern (northern) boundary was shifted to the north (south), whereas both the eastern and western boundary were slightly shifted to the west. It should be noted that, both D1 and D3 used in this study are indeed selected based on early study using Eta operational model by Xue et al. (2007), with D1 and D3 being identical to their big domain and small domain, respectively.

Time-dependent initial and LBCs necessary to run NMM/SSiB3 for a scenario case over a specific domain were obtained from the same GFS/SSiB2 scenario case. For example, the GFS/SSiB2 Case SUBT for March 31st, 2015, was used as the NMM/SSiB3 initial and LBCs to generate the corresponding NMM/SSiB3 Case SUBT over a selected domain, which also was integrated starting from March 31st, 2015. All NMM/SSiB3 experiments, were completed using a one-way nesting (NMM/SSiB3 has no feedback to GFS/SSiB2), and the time period for our NMM/SSiB3 scenario cases simulations are also similar to those of the corresponding driving GFS/SSiB2 scenario cases. Furthermore, since this paper focuses on the effects of different factors on the LST/SUBT dynamical downscaling ability, all RCM experiments do not use spectral nudging techniques. Note that the NMM/SSiB3 Case SUBT experiments with D1, D2, and D3 are referred to as NMM/SSiB3 Case SUBT followed by "D1" or "D2" or "D3", to indicate the selected domain. For instance the NMM/SSiB3 Case SUBT completed over D3 will be labeled NMM/SSiB3_D3 Case SUBT, (see Table 2 for details). Figure S2 demonstrates that all the NMM/SSiB3 Case SUBT simulations indeed produce reasonably the observed May 2015 precipitation, though some dry/wet biases are still evident. For instance, for the precipitation (see Figure S2), the spatial correlation between different NMM/SSiB3, GFS/SSiB2 simulation and the GTS observation over the SGP are 0.69, 0.84, 0.71, and 0.79 for GFS/SSiB2 Case SUBT, NMM/SSIB3_D1 Case SUBT, NMM/SSIB3_D2 Case SUBT, and NMM/SSIB3_D3 Case SUBT, respectively. Similarly to the precipitation, all simulations reproduce the observed 2 m-temperature spatial distribution,

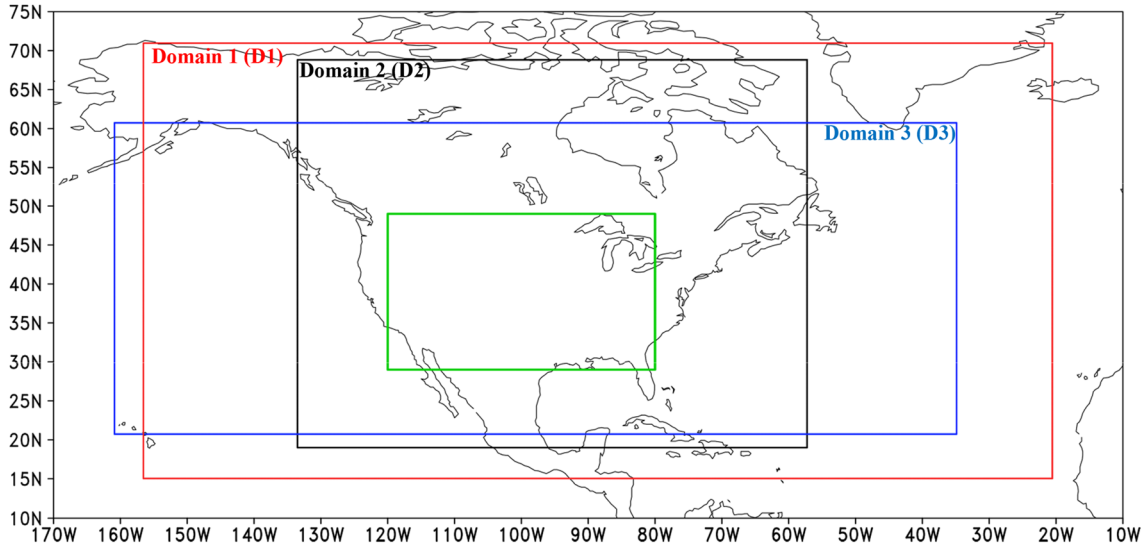

Fig. 1 Domains used for the weather research and forecasting (WRF) model simulations. Domains of configurations D1, D2, and D3 for NMM/SSiB3 are delimited by red box, black box and blue box, respectively. The innermost box represents the "Test area" [hereafter whole USA or Common Validation Areas (CVA); 80°W–120°W and 29°N–49°N], for which statistic measures are computed

Table 2 Initial SUBT and NMM/SSiB3, ARW/SSiB3 and NMM/SSiB2 lateral boundary conditions for the two scenario cases over different domains

Model	Scenario cases	Initial SUBT and LBCs for NMM/SSiB3	Description
GFS/SSiB2	GFS/SSiB2 Case SUBT	Imposed SUBT anomaly for 1st time step (see Figure S1 for the anomaly)	GFS/SSiB2 control case
	GFS/SSiB2 Case noSUBT	No-imposed anomaly for 1st time step	
NMM/SSiB3 over domain 1	NMM/SSiB3_D1 Case SUBT	GFS/SSiB2 Case SUBT	NMM/SSiB3 control case over domain 1
	NMM/SSiB3_D1 Case noSUBT	GFS/SSiB2 Case noSUBT	
NMM/SSiB3 over domain 2	NMM/SSiB3_D2 Case SUBT	GFS/SSiB2 Case SUBT	NMM/SSiB3 control case over domain 2
	NMM/SSiB3_D2 Case noSUBT	GFS/SSiB2 Case noSUBT	
NMM/SSiB3 over domain 3	NMM/SSiB3_D3 Case SUBT	GFS/SSiB2 Case SUBT	NMM/SSiB3 control case over domain 3
	NMM/SSiB3_D3 Case noSUBT	GFS/SSiB2 Case noSUBT	
ARW/SSiB3 over domain 3	ARW/SSiB3 Case SUBT	GFS/SSiB2 Case SUBT	ARW/SSiB3 control case over domain 3
	ARW/SSiB3 Case noSUBT	GFS/SSiB2 Case noSUBT	
NMM/SSiB2 over domain 3	NMM/SSiB2 Case SUBT	GFS/SSiB2 Case SUBT	NMM/SSiB2 control case over domain 3
	NMM/SSiB2 Case noSUBT	GFS/SSiB2 Case noSUBT	

Each scenario cases in this study consisted of seven (7) ensemble members with different initial conditions from March 27, 2015 to April 02, 2015

with spatial correlation over the western US exceeding 0.81 in all control cases (see Figure S3).

Since the difference between GFS/SSiB2 Case SUBT and GFS/SSiB2 Case noSUBT are solely attributed to the imposed warm initial LST/SUBT anomaly (see Table 2), the difference between GFS/SSiB2 Case SUBT and GFS/SSiB2 Case noSUBT allows us to isolate the potential effect of the LST/SUBT on the May 2015 flooding over the SGP. For convenience here, the difference between GFS/SSiB2 Case SUBT and GFS/SSiB2 Case noSUBT (GFS/SSiB2 Case SUBT minus GFS/SSiB2 Case noSUBT) will be henceforth referred to as Case GCM (see Table 3). Similar to GFS/SSiB2, the differences between two NMM/SSiB3 scenarios cases over a specific domain, for instance NMM/SSiB3_D1 Case SUBT and NMM/SSiB3_D1 Case noSUBT, should provide information on how influential the SUBT/LST was on the May 2015 SGP flooding when considering that domain. The differences between two NMM/SSiB3 scenario cases achieved over specific domains are henceforth labeled as Case D1, Case D2, and Case D3, where "D1", "D2", and

Table 3 Acronyms and definition of the different cases used to show the effect of the SUBT for May 2015

Cases	Model used	Description of different cases
OBS	CAMS/CPC/NARR	May 2015 anomaly is generated from the 1986–2015 May climatology period
Case GCM	GFS/SSiB2	*Case GCM* represents the difference between the GFS/SSiB2 control case (GFS/SSiB2 Case SUBT) and GFS/SSiB2 Case noSUBT, i.e. GFS/SSiB2 Case SUBT minus GFS/SSiB2 Case noSUBT
Case D1	NMM/SSiB3 over domain 1 (D1)	*Case D1* represents the difference between the NMM/SSiB3 control case over D1 (NMM/SSiB3_D1 Case SUBT) and NMM/SSiB3_D1 Case noSUBT, i.e. NMM/SSiB3_D1 Case SUBT minus NMM/SSiB3_D1 Case noSUBT
Case D2	NMM/SSiB3 over domain 2 (D2)	*Case D2* represents the difference between the NMM/SSiB3 control case over D2 (NMM/SSiB3_D2 Case SUBT) and NMM/SSiB3_D2 Case noSUBT, i.e. NMM/SSiB3_D2 Case SUBT minus NMM/SSiB3_D2 Case noSUBT
Case D3	NMM/SSiB3 over domain 3 (D3)	*Case D3* represents the difference between the NMM/SSiB3 control case over D3 (NMM/SSiB3_D3 Case SUBT) and NMM/SSiB3_D1 Case noSUBT, i.e. NMM/SSiB3_D3 Case SUBT minus NMM/SSiB3_D3 Case noSUBT

Here, Case GCM, Case D1, Case D2, and Case D3 show the SUBT/LST effect on the GFS/SSiB2 and the different NMM/SSiB3 results. Comparisons between Case D1, Case D2, and Case D3 emphasize the sensitivity to the choice of domain sizes and boundary locations

"D3" indicate the domain employed, respectively. We recall the different cases, Case D1, Case D2, and Case D3, are designed to evaluate the impact of simulated SUBT/LST response to different domain sizes and boundary conditions location, along with the sensitivity of simulated precipitation and associated large-scale features to the SUBT/LST effect (see Table 3).

Regional climate models' abilities in intra-seasonal and seasonal simulations/predictions have been found to be sensitive to many factors including dynamic cores and land-surface process parameterizations (see reviews by Xue et al. 2014; Giorgi and Gutowsky 2016). In order to investigate the effect of change in dynamic core within the same model, we also used the ARW/SSiB3 and executed two sets of experiments scenarios driven by the corresponding GFS/SSiB2 scenarios over D3. The choice of D3, as will be discussed later in Sect. 3.1, is because we have identified D3 as an optimum domain size with the better simulation of the LST/SUBT downstream effects in North America. The experiments with imposed warm initial LST/SUBT anomalies (CTRL) and no imposed warm anomalies are referred to as ARW/SSiB3 Case SUBT and ARW/SSiB3 Case noSUBT, respectively. For convenience here, the difference between ARW/SSiB3 Case SUBT and ARW/SSiB3 Case noSUBT (i.e. ARW/SSiB3 Case SUBT minus ARW/SSiB3 Case noSUBT) henceforth will be referred to as Case C3.

In addition to the investigation of the sensitivity of the SGP precipitation anomaly to change in dynamical core within the same model, we also explore how different surface process parameterization affects the precipitation anomaly over the SGP due to warm LST/SUBT over the WUS. Here we used over D3 the NMM/SSiB2 in both the control run (NMM/SSiB2 Case SUBT) and no-imposed anomaly runs (NMM/SSiB2 Case noSUBT). The difference between NMM/SSiB2 Case SUBT and NMM/SSiB2 Case noSUBT (NMM/SSiB2 Case SUBT minus NMM/SSiB2 Case noSUBT) is labeled as Case S3. All the details of the experimental design for dynamic cores and land surface condition changes are also described in Tables 1 and 2, while Table 4 lists their differences compared respectively to Case D3.

2.3 Validation datasets and methodology

To evaluate the simulated effect of LST/SUBT in different cases, we have used various types of datasets (gauge-observations and reanalysis). For precipitation, we used the 0.25° x 0.25° latitude/longitude gauge-based observed daily precipitation from the National Oceanic and Atmospheric Administration (NOAA) Climate Prediction Center (CPC), which provides over the contiguous United States (CONUS) domain a long-term and high-resolution record of daily precipitation (Chen et al. 2008). For the near-surface temperature (T2m), we used the Global Historical Climatology Network version 2 and the Climate Anomaly Monitoring System (GHCN-CAMS) gauge-based 2-m temperature over land, which provides global coverage of monthly means on a regular resolution of 0.5° latitude x 0.5° longitude grids (Fan and van den Dool 2008). In addition, for large-scale environmental conditions analysis, such as vertically integrated moisture flux, geopotential height, relative humidity, and wind fields, we used the NCEP North American Regional Reanalysis (NARR) climate datasets with horizontal resolution of 32 km and 45-layer at vertical resolution over the North American domain (Mesinger et al. 2006). We used the 500-hPa geopotential height to depict the North Atlantic Subtropical High (NASH) and the 925-hPa meridional wind for the SGP Low Level Jet (LLJ). The CPC and GHCN-CAMS are available from 1948 to present, while NARR is available from 1979 to near present. We generate the anomaly for these datasets from the climatology based on the period from 1986 to 2015, following the same 'benchmark' selection method discussed by Xue et al. (2018).

Table 4 Summary of the Case D3, Case C3, and Case S3 model configuration differences

Case labeling	Dynamic core	Land Surface Scheme	Definition of the case	Note for comparison
Case D3	NMM	SSiB3	Case D3 represents the difference between NMM/SSiB3_D3 Case SUBT and NMM/SSiB3_D3 Case noSUBT	
Case C3	ARW	SSiB3	Case C3 represents the difference between ARW/SSiB3 Case SUBT and ARW/SSiB3 Case noSUBT	Comparison between Case D3 and this case (Case C3) shows the change in dynamic core effects
Case S3	NMM	SSiB2	Case S3 represents the difference between NMM/SSiB2 Case SUBT and NMM/SSiB2 Case noSUBT	Comparison between Case D3 and this case (Case S3) shows the land surface parameterization effects

Similar domain (Domain 3), were utilized to generate Case D3, Case C3 and Case S3

We should mention that, for the analysis presented in this paper, particularly Sect. 3.1, we mostly focus our analysis of near surface temperature, precipitation, and large-scale environmental conditions on May 2015 because it was the month with an unusual amount of precipitation, causing severe flood damage with large socio-economic impacts over Texas and adjoining areas, namely the SGP. The May 2015 anomaly (as a departure from the 1986–2015 mean) obtained from those data will then serve as observational reference (benchmark) for comparison against the model-simulated Case GCM, Case D1, Case D2, and Case D3 to verify the LST/SUBT effect on the abnormal high precipitation over the SGP, along with the sensitivity to domain size choice and boundary positions. To avoid confusion, the aforementioned anomaly either from observations (GTS and CAMS) or reanalysis (NARR) will be henceforward named as OBS. For analysis and comparison purposes, we also defined a common verification area (CVA), namely also referred to as "whole USA" and covering almost all CONUS land point. The CVA ("whole USA") is defined as a longitude-latitude rectangle bounded from 120°W to 80°W and 29°N to 49°N as shown in Fig. 1. Please note that, since Case D3, Case C3, and Case S3 utilize similar domain size, we evaluate the effect of: (1) the change in dynamic core by comparing Case D3 and Case C3, and (2) the effect of surface process representation by comparing Case D3 and Case S3. The main differences between these cases are summarized in Table 4, and a detailed discussion of these results will be presented in Sects. 3.2, and 3.3 respectively.

3 Results and discussions

3.1 Domain size and boundary location

Figure 2 displays the 2-m temperature anomalies in May 2015 from OBS, Case GCM, Case D1, Case D2, and Case D3. The OBS displays two areas of positive temperature anomalies, one over half of the northwestern US from Central California to Washington State, where anomalies mainly range between 1 and 3 °C. As depicted in Fig. 2a, this area is dominated by the Rocky Mountains and covers the region between 124.5°W–110°W and 35°N–50°N. A second area of considerably warm T2m anomalies ranging from 0.5 to 4 °C can be seen over the eastern half of the CONUS. A region of negative T2m anomalies in the range between − 1 and − 3 °C separates these two regions. This cold region is mainly located along the Great Plains region, from New Mexico to Southern Montana. Case GCM simulates the magnitude and extension of the warm temperature anomaly over the WUS, but does not fully capture the magnitude of the warm anomaly. The second warm anomaly located over the eastern half of the CONUS in the OBS is missing in

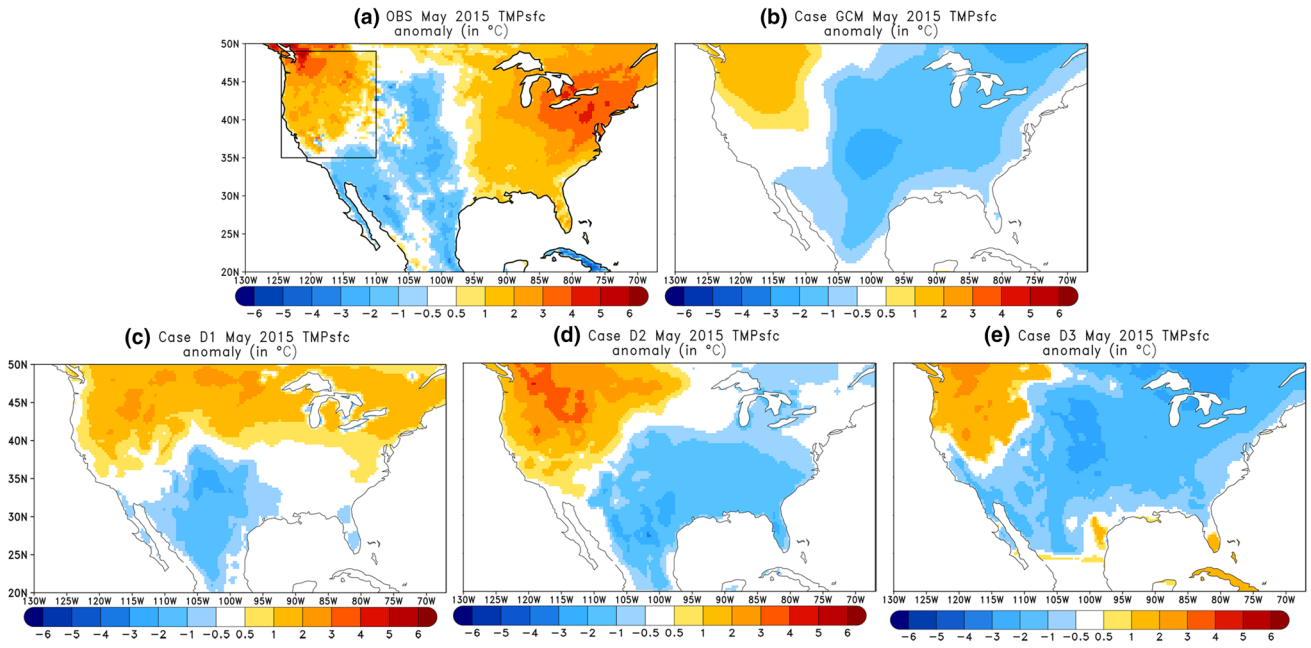

Fig. 2 May 2015 Observed (CAMS observation) and simulated land surface temperature (LST; unit: °C) anomalies over United States. **a** CAMS LST difference between May 2015 and the 1986–2015 climatology. **b–e** the corresponding simulated LST anomalies from Case GCM, Case D1, Case D2, and Case D3, respectively. The black box in **a** indicates the Western United States (WUS; 110°W–124.5°W and 35°N–49°N) considered in this study

Case GCM. In addition, Case GCM overestimates the cold anomaly with somewhat of an extension toward the eastern coast, resulting in a low spatial correlation coefficient (PCC; 0.17) with OBS and high root mean square error (RMSE; 2.06) over the whole USA. Upon analyzing the RCM cases, we found that Case D1, Case D2, and Case D3 (Fig. 2c–e, respectively) produced adequate spatial distribution of Case GCM T2m anomalies, in particular the warm temperature anomaly over the WUS and the cold anomaly over the Southern Plains, a region stretching between 25°N-45°N latitudes in all domains with high spatial correlations over the WUS (exceeding 0.7) and an absolute bias of less than 0.4 °C. Indeed, despite sharing many resemblances, Case D1, Case D2, and Case D3 do exhibit significant localized differences as displayed in Fig. 2c-e, with, however, only Case D1 being able to reproduce the observed warm anomaly over the Midwest and Northeast. The WUS area average temperature anomalies for Case D1, Case D2, and Case D3 are, respectively, 1.03, 1.80, and 1.12 °C, while the average RMSE values over the whole USA range from 1.40 to 2.04 °C, with lowest RMSE (1.40 °C) obtained from Case D3. Note that the observed warm temperature anomaly over the WUS region is 1.30 °C, emphasizing that Case D3 produces the best temperature anomalies over the WUS, thereby indicating a better level of agreement with OBS in the WUS temperature pattern. Although all RCM cases reproduce the positive anomaly over the WUS, with Case D2 and Case D3 being more comparable with Case GCM, there exists a clear difference in temperature anomaly magnitude and extent between the RCM cases with different domains. This suggests that the temperature distribution of a sub-region within the RCM domain is sensitive to the domain size. The following discussion will show that the warm LST anomalies in the WUS are likely to be in part responsible for the May 2015 SGP flood's development.

Figure 3 displays the corresponding distribution of precipitation anomalies from OBS, Case GCM, Case D1, Case D2, and Case D3. In Fig. 3b-e, the dots correspond to differences that are significant at 90% confidence levels, as determined by a Student's t test. The OBS shows a band of maximum precipitation anomaly (4–6 mm/day) in May 2015 over the Southern Great Plains and surrounding areas, from Texas to Louisiana, Arkansas, and Oklahoma and regions to the northwest, whilst a dry precipitation anomaly (between − 1 and − 3 mm/day) is depicted over the east and extends from the eastern edge of Mississippi and Alabama to Kentucky where it peaks (Fig. 3a). Though Case GCM is able to reproduce a statistically significant wet precipitation anomaly pattern over the heavy rainfall regions, such as Texas and Oklahoma, the rainfall anomaly has been overestimated by 1.5–3 mm/day over the south-eastern US (between 85°W–75°W and 28°N–40°N) and underestimated by 0.5–2 mm/day over the Rockies and in some areas toward west of the Great Lakes (Fig. 3b). Compared with Case GCM, Case D1, Case D2, and Case D3 (Fig. 3c–e) indeed reasonably produced the main geographical features, in particular the east–west contrast gradient, though with a weaker intensity. For instance, Case D1 underestimated the observed

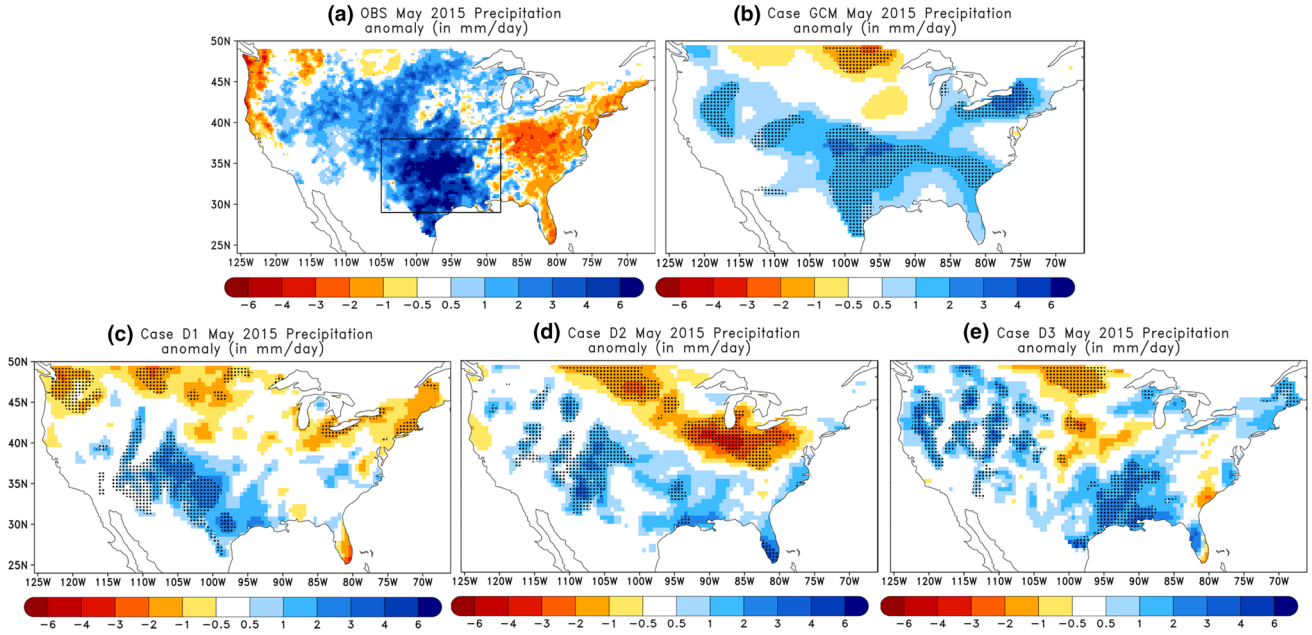

Fig. 3 Same as Fig. 2, except showing precipitation (unit: mm/day) results, where observations (OBS) are represented by GTS. Black boxed region in **a** indicates the Southern Great Plains and adjacent areas (labeled SGP; 88°W–105°W and 29°N–38°N) used in this study. The stippled (dotted) areas denote the areas statistically significant at a 90% confidence level

rainfall excess pattern across Louisiana and Arkansas, whereas Case D2 over-predicted the rainfall deficit across the southern Great Lakes but replicated with better accuracy the positive rainfall anomaly regionally over the SGP and neighboring areas. We also noticed that, Case D1 and Case D2 are dryer than OBS over most of the CONUS resulting, respectively, in a mean bias of − 1.13 and − 1.21 mm/day, respectively and a RMSE ranging from 2.17 (Case D1) to 2.42 (Case D2). The under-prediction of precipitation over the CONUS, in particular the SGP, seems to be a common weakness of many regional climate models (Xue et al. 2007, 2016; Mearns et al. 2012; De Sales and Xue 2013; Saini et al. 2016; Sun et al. 2016). Recently, Hu et al. (2018) suggested the spectral nudging approach as an effective solution to alleviate the precipitation dry bias. In opposition to Case D1 and Case D2, the dryness is somewhat reduced in both spatial extent and magnitude in Case D3, leading to a better simulation of the anomalous positive precipitation over the SGP (32% of observed anomaly) due to the LST/SUBT effect, in agreement with the more accurate simulation of the WUS positive land surface temperature anomaly (see Fig. 2). The results in this study confirm that a reasonably good simulation of observed WUS LST anomaly is necessary for a more accurate simulation of the SGP extreme precipitation response due to the LST/SUBT effect, but the simulated precipitation anomaly is largely sensitive to the domain size choice and boundary locations.

Overall, notwithstanding the domain choice, it can be seen in all simulation cases analyzed in this study that, the observed positive rainfall/temperature anomalies over the SGP/WUS are well captured, although we noticed a wide spread and variation in the magnitude of anomaly. The large spread of simulated surface temperature and precipitation anomalies over the WUS and SGP, respectively, were also reflected in the May 2015 regional averages of both surface temperature and precipitation (Table 5). In addition, all RCM cases capture the observed dry conditions in some parts/regions of the south-eastern US, while the simulated wet anomaly in the driving GCM case (Case GCM) probably due to stronger vertical motion (not shown), was inconsistent with the observed drought there, thereby emphasizing the added value of the dynamical downscaling for better simulations of local/regional and meso-scale processes (e.g. De Sales and Xue 2013; Xue et al. 2014; Diallo et al. 2016, 2018). Our results confirm that the spring WUS LST/SUBT anomaly plays a significant role in the development of the late spring SGP extreme precipitation. More specifically, the warm spring LST anomalies in the WUS are likely to be in part responsible for the SGP May 2015 flood's development. However, the abnormal rainfall magnitude and spatial location extent over the SGP, along with the WUS LST anomalies, are sensitive to the domain size choice and boundary position. In fact, we note that although Case D1, Case D2, and Case D3 share many resemblances to each other, the more realistic simulation of the positive precipitation anomaly over the SGP is achieved when reducing D1 to D3, emphasizing the importance of the southern boundary location. This is consistent with the previous study (Xue et al. 2007) that pointed out that the North American climate simulation was particularly sensitive to the southern boundary location in the Gulf of Mexico and the Caribbean Sea. We should note that, the assessments for the LST/SUBT effect here are likely affected by the models weaknesses/errors. Additionally, it is worth pointing out that, this factor (LST/SUBT) as well as others elements such as SST (Xue et al. 2018), soil moisture (Xue et al. 2004; Koster et al. 2016; Saini et al. 2016), vegetation (Xue et al. 1996; Bamba et al. 2018), and atmospheric internal variability (Seager et al. 2014; Lee et al. 2018) may have also contributed to the observed anomaly. Jee and Kim (2017) analyzed the influence of spin up time using the WRF version 3.6 on the simulation of heavy rainfall over Seoul and its adjacent cities. They concluded that their precipitation simulations were affected by the spin-up time and short spin-up time produced a more accurate distribution of precipitation intensity than the other experiments. In our numerical experiments, we have shown that the RCM DDM of the LST/SUBT downstream effect in North America is sensitive to the domain size choice and boundary condition location. However, the effect of spin-up time on the relationship between LST/SUBT anomalies over WUS and downstream precipitation anomaly in North America remains an open question.

The precipitation over the SGP in late spring/summer is more governed by large-scale dynamical features forcing, such as the North Atlantic Subtropical High (NASH), along with the atmospheric stationary wave extending eastward from the WUS and the Great Plains Low Level Jet (GPLLJ) (Chang and Wallace 1987; Weaver et al. 2009; Cook et al. 2008; Saini et al. 2016; Harding and Snyder 2015; Patricola et al. 2015; Xue et al. 2007, 2012, 2016, 2018; Ryu and Hayhoe 2017; and references cited therein). Hereby, diagnosing

Table 5 Mean and spatial correlation coefficient (PCC) of May 2015 precipitation and 2-m temperature anomalies averaged over the SGP (88°W–105°W and 29°N–38°N) and western US (110°W–124.5°W and 35°N–49°N), respectively

Metrics	Precipitation (in mm/day)		Temperature (in DegC)	
	Mean	PCC	Mean	PCC
OBS	3.72		1.31	
Case D1	0.86 (23%)	0.06	1.80	0.60
Case D2	1.08 (29%)	0.29	1.03	0.45
Case D3	**1.20** (**32%**)	**0.38**	**1.12**	**0.87**

Units: Precipitation in mm/day and 2-m temperature in °C. Highlighted numbers using bold indicate better performance

the root causes behind these differences in the rainfall anomaly simulations due to the choice of domain sizes impels us to further explore into the simulated large-scale dynamic features to understand the underlying mechanisms.

The spring LST/SUBT anomalies in the Western US effects on the downstream precipitation anomaly in North America are associated with a large-scale stationary wave from the LST anomaly area ("heated area") and extending eastward (Xue et al. 2012, 2018). The warm temperature anomaly in the west heats the surface as well as low and middle troposphere through sensible heat flux and produces an anomalous positive geopotential height in the middle troposphere (500 hPa), inducing an anomalous planetary wave train across North America. In the following sections, we quantitatively evaluate the LST/SUBT effects of different domain size on the key atmospheric circulations that drive SGP precipitation.

Figure 4 displays the May 2015 geopotential height anomaly at 500 hPa from Case GCM, Case D1, Case D2 and Case D3 as well as its comparison with OBS. The corresponding meridional wind (V component of the wind; V-wind) speed anomaly at 925-hPa (the core level of the SGP LLJ) is displayed in Fig. 5. OBS shows an increase in the strength of the SGP LLJ with the core of maximum anomaly (2–4 m/s) located over the SGP (between 29°N and 34°N) (Fig. 5a). At the same time, the geopotential height is characterized by a negative anomaly over the Western US through southern Mexico and a positive anomaly extended over Central and Eastern US from the Atlantic (Fig. 5a). The enhancement of the SGP LLJ, together with the anomalous high pressure over the southern Atlantic, drives moisture transport from the Gulf of Mexico into the SGP, which in turn contributes to high precipitation over the SGP (Figs. 3a, 4a). Case GCM simulates the dipole pattern for the anomalous geopotential height (Fig. 4b) across the CONUS. But Case GCM does not fully capture the spatial patterns and magnitudes of the anomalies. It has to be noted that Case GCM shows a large discrepancies in the representation of the anomalous geopotential height compared to the OBS. Among the discrepancy, the negative (positive) anomaly is displaced south (east) in case GCM compared to OBS, but as we mentioned earlier in addition to the LST/SUBT other factors has contributed to the observed anomaly. Please note that, when summing up the LST/SUBT effect and the SST effect from the GCM, our simulation succeeds to replicate adequately the OBS (NARR reanalysis) geopotentiel height anomalous pattern, including location and magnitude, particularly the positive anomalies over Alaska and southeast US as well as the negative anomalies north of Midwest and west US (not shown). In case GCM, the SGP LLJ strengthening is also shifted far eastward compared to OBS. This eastward shift is consistent with the simulated moisture flux (see discussion of Fig. 6b) and may explain why the Case GCM produced wet precipitation anomalies (Fig. 3b) over south-east United States. Conversely,

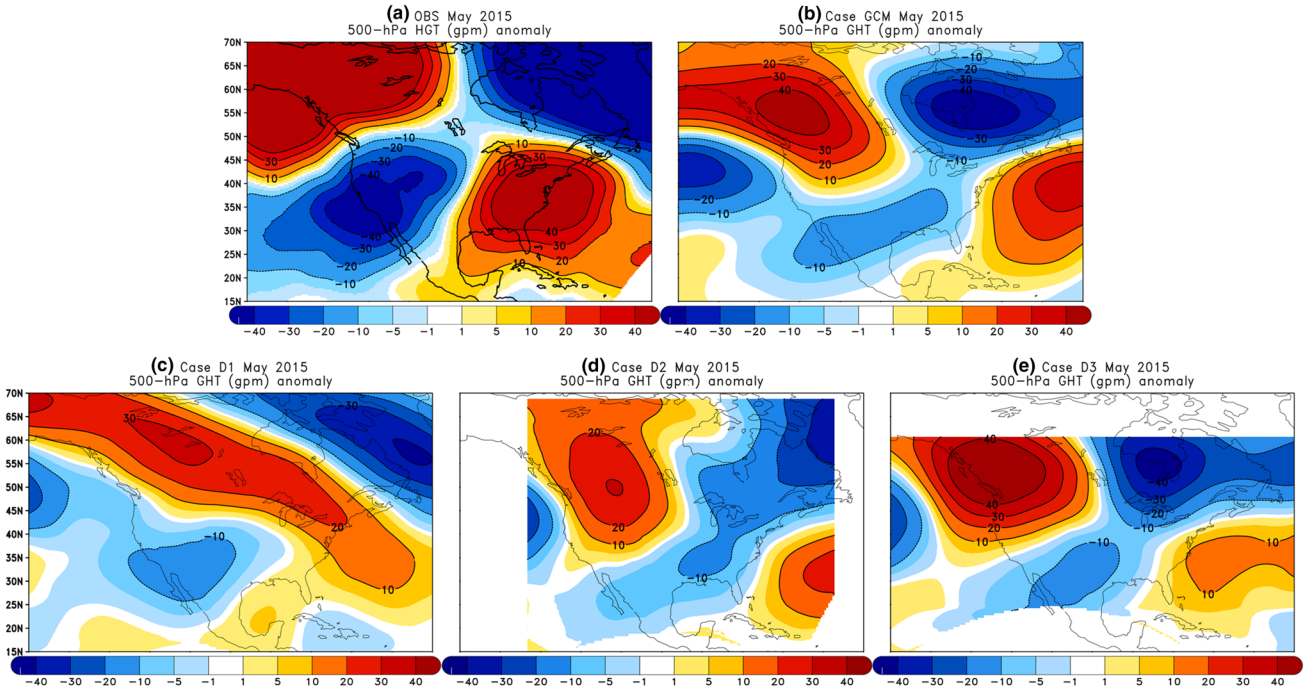

Fig. 4 May 2015 500-hPa geopotential height (contours, unit: gpm) anomaly from: **a** OBS (NARR reanalysis), **b** Case GCM, **c** Case D1, **d** Case D2, and **e** Case D3

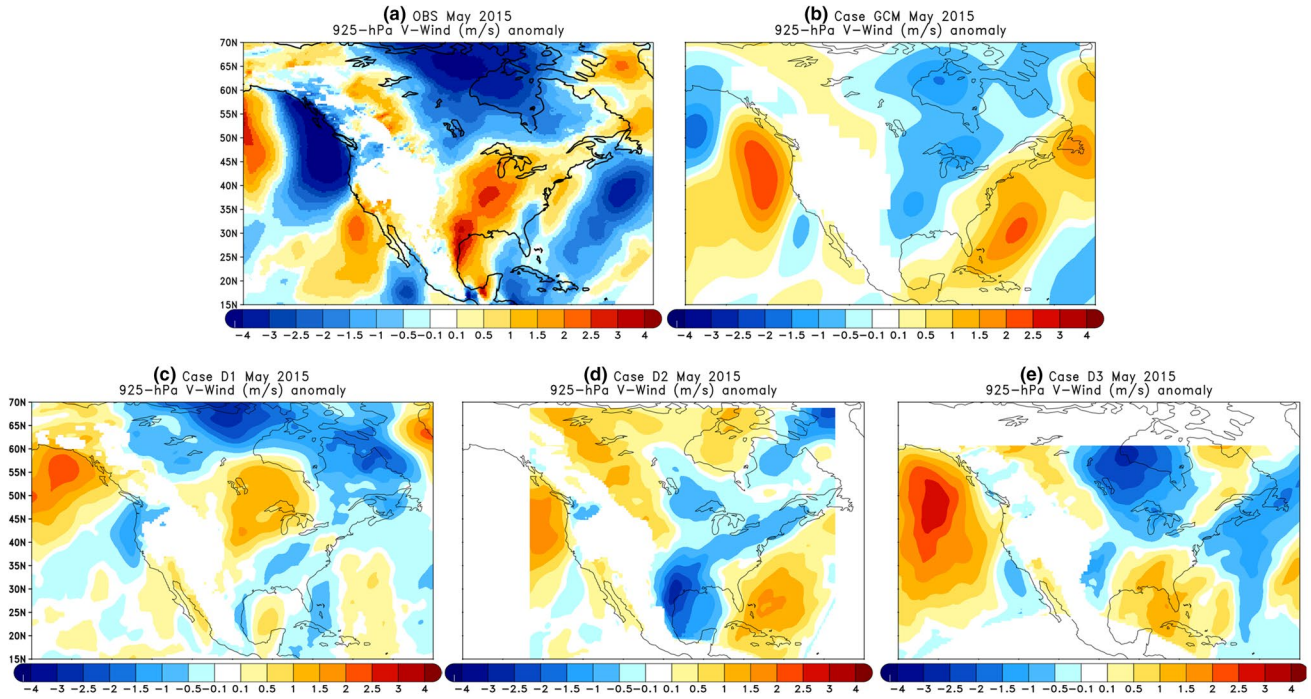

Fig. 5 Same as Fig. 4, but for the 925-hPa meridional wind (925-hPa; V-Wind). Unit: m/s

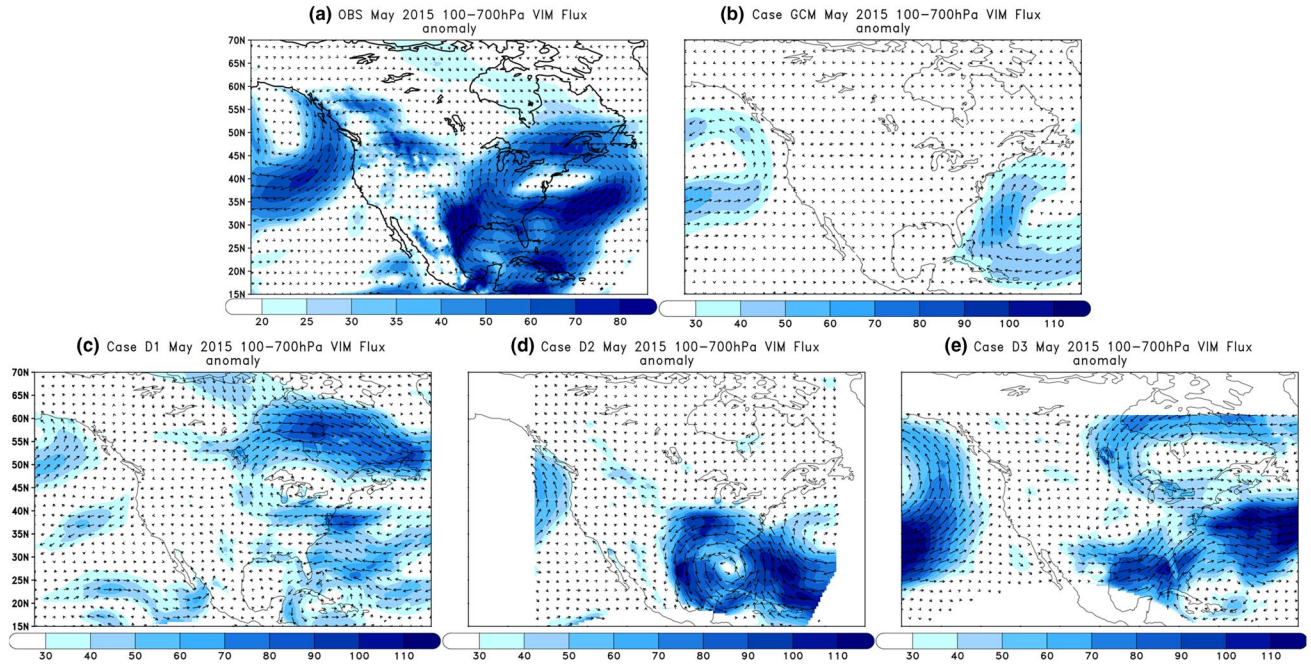

Fig. 6 Same as Fig. 4, except showing the 1000–700 hPa vertically integrated moisture flux (vectors, units: g/kg m/s) anomaly superimposed with its moisture transport (shaded, unit: g/kg m/s) anomaly

Case D1 and Case D2 clearly exhibit a weakening of the LLJ over the SGP. Additionally, Case D3 shows a negative geopotential height anomaly centered over the SGP, while Case D1 shows a positive geopotential height anomaly extended from the Atlantic to Canada. Overall, Case D3 has downscaled with good accuracy the Case GCM wave train across North America (Fig. 4e) and replicated reasonably the location of the SGP LLJ maximum. These

results indeed, further highlight that the simulated large scale-structures due to LST/SUBT effect are largely sensitive to the domain size.

The May 2015 moisture flux anomalies from OBS, Case GCM, Case D1, Case D2, and Case D3 are shown in Fig. 6. The moisture flux is integrated between 1000 and 700 hPa. OBS shows the strong major moisture transport was extended toward the north of the Great Lakes. In May 2015, there were large moisture flux anomalies transported through the Gulf of Mexico from the North Atlantic to the CONUS. In Case GCM, the moisture transport from the Gulf of Mexico toward the SGP region is weaker, with the most prominent difference being the eastward displacement of the core of high moisture flux values off the east coast (Fig. 6b), contributing to more precipitation there. Case D1 and Case D2 showed a large moisture flux anomaly over the SGP compared with Case GCM, but such moisture was being drawn out from the SGP regions toward the Gulf of Mexico (Fig. 6c, d), which was consistent with the simulated lower SGP precipitation (Fig. 3c, d) anomaly. The moisture flux anomalies in Case D3, however, are much closer to those in OBS, in particular the moisture moving from the Gulf of Mexico toward the SGP region, consistent with its high relative humidity and precipitation anomalies (see Figs. 3e, 7e).

Figure 7 illustrates the 850-hPa simulated May 2015 relative humidity (RH) anomalies by Case GCM, Case D1, Case D2, and Case D3 as well their comparison with OBS. Figure 7a shows that May 2015 RH anomalies at 850 hPa from OBS have the largest positive RH (approximately 12–20%), mostly located off the West Coast as well as over the Great Plains region and Southern Rockies where the observed heavy precipitation anomaly band was located. The negative RH (−4 to −6%) in OBS is localized over the southeastern United States and east of the Great Lakes, which corresponds well with the below-normal precipitation area shown in Fig. 3a. Figure 7b-e indicate that all cases reasonably capture the overall spatial distribution of relative humidity anomalies, although somewhat significant localized differences do occur. Compared to OBS, Case GCM simulates the significant positive RH off the West Coast but does not properly replicate the negative RH over the Southeastern United States. The May 2015 relative humidity anomaly over the CVA for OBS and Case GCM, Case D1, Case D2, and Case D3 are 5.7, 2.09, 0.50, 1.88, and 3.48, respectively. The most prominent differences between Case D1 and Case GCM and between Case D2 and Case GCM are identically positive RH anomalies over the Gulf of Mexico. These suggest that changing D1–D2 does not significantly affect the RH anomaly simulations because in these domains the north–south simulated temperature gradient was not substantially different. Since moisture transport from the Gulf of Mexico is the major source of moisture for the SGP, the above suggests that the extended D1 and D2 decrease the moisture supply to the SGP and thereby weaken its associated precipitation, consistent with the low precipitation in Cases D1 and D2. However, Case D3 adequately produced

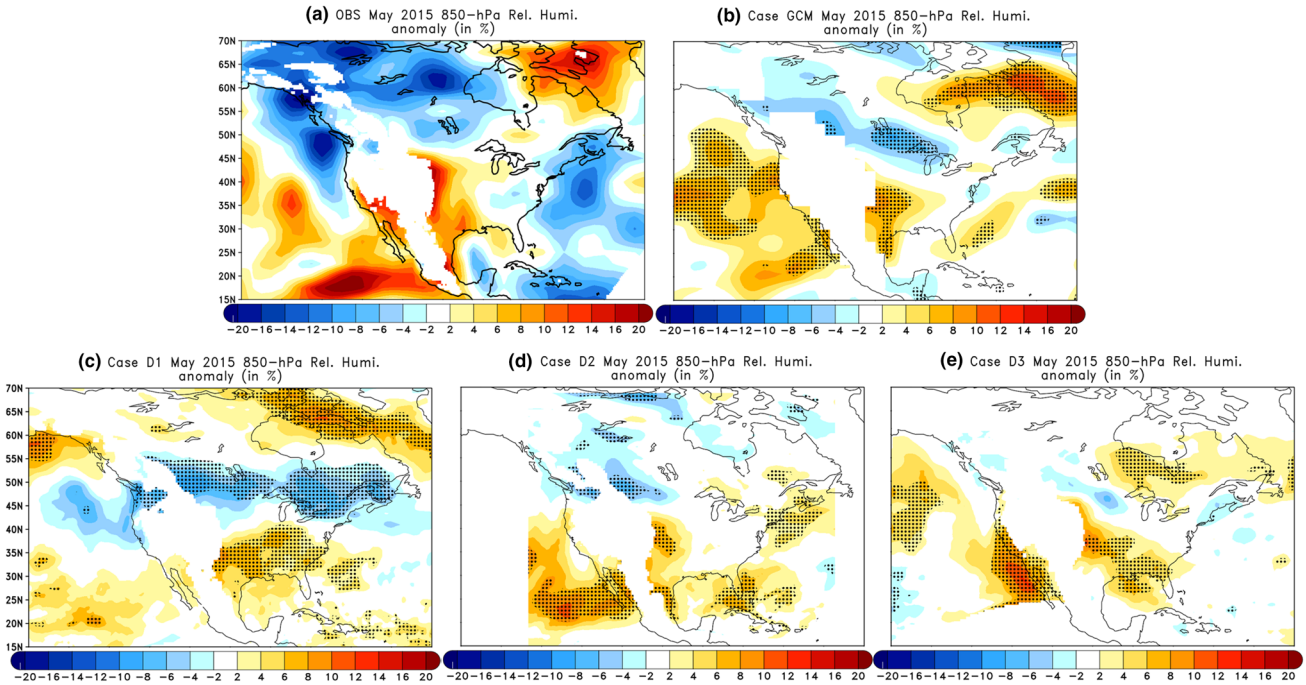

Fig. 7 May 2015 850-hPa relative humidity (RH, unit: %) from: **a** OBS, **b–e** Case GCM, Case D1, Case D2 and Case D3, respectively. The stippled (dotted) areas denote the areas statistically significant at a 90% confidence level

the observed precipitation anomaly, along with largely corrected the positive/negative RH in both Case D1 and Case D2 over the south-eastern US (Fig. 7e), suggesting that the CONUS means climate simulation as well as the RCM DDM of the LST/SUBT downstream effect are particularly sensitive to the southern boundary location.

In summary, an appropriate location of the southern boundary position is a key element for an accurate simulation of mean precipitation anomaly over the SGP, along with associated eastward wave train features induced by the LST/SUBT downstream effect. The southern boundary location has been identified to be crucial in producing the SGP Low Level Jet strength together with the increased southerly component of the water vapor fluxes that transport moisture into the Southern Great Plains from the Gulf of Mexico and thereby result in a better (quantitatively and regionally) simulation of the precipitation anomaly over the SGP. Consequently, the choice of the domain size for the LST/SUBT downstream effect investigation in North America is of critical importance and should be selected with caution, whereby on the one hand to account for the main large-scale processes including the humidity source of the Gulf of Mexico and on the other hand to include the planetary wave genesis region.

3.2 Impact of WRF dynamic core

In this section we explore the sensitivity of the DDM for the LST/SUBT downstream effect to change in dynamical core within the same model. Case C3 and Case D3 are generated using different dynamic cores: the ARW and NMM, respectively. Figure 8a-b display the sensible heat flux anomaly (positive values indicate an upward flux) for the first 10 days

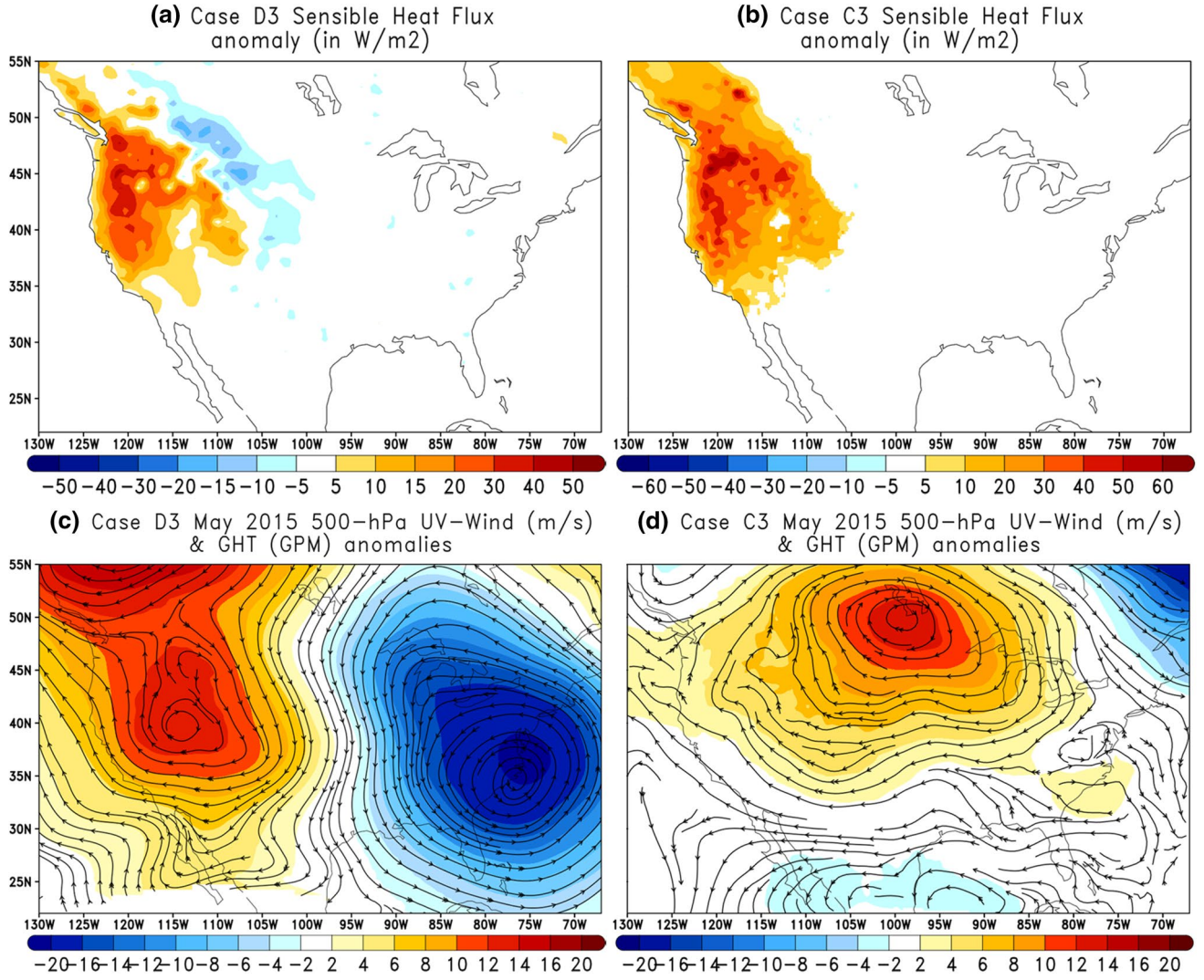

Fig. 8 Simulated sensible heat flux (unit: W/m^2) differences for the first 10 days from: **a** Case D3 and **b** Case C3. **c** Same as **a** but for the 500-hPa geopotential height (shaded, unit: gpm) superimposed with the 500-hPa wind direction (streamlines, unit: m/s). **d** Same as **c** but for Case C3

of integration from Case D3 and Case C3, respectively. Both dynamical cores exhibit a positive sensible heat flux anomaly over the WUS and part of Canada from Southern California, which resulted from the initial imposed warm LST/SUBT anomaly over the WUS. Note that, the most prominent difference between Case D3 and Case C3 is the negative sensible heat flux anomaly (5–15 W/m^2) outside the WUS. In Case D3, it is clear that the positive sensible heat flux anomaly over the WUS induces a strong positive geopotential height anomaly in the middle troposphere (500 hPa) over western North America, which in turn produces a strong anti-cyclonic circulation (Fig. 8c), which has been proposed as a mechanism for the LST/SUBT downstream effects on floods in North America as discussed in details by Xue et al. (2018). On the other hand, although Case C3 has simulated the positive sensible heat flux anomaly over the WUS, the core of strong positive geopotential height anomaly, along with the strong anti-cyclonic circulation, however, are shifted to the upper Midwest (Fig. 8d). Indeed, these strong anti-cyclonic circulation patterns over the upper Midwest will favor a weakening of the rising motion and thus reduce the likelihood and amount of late spring rainfall anomaly over the SGP. Additionally, Case C3 misses the negative geopotential height anomaly in eastern North America, indicating that the wave train across North America induced by the WUS LST/SUBT anomaly is sensitive to the dynamic processes. Litta et al. (2012) used the NMM and ARW dynamical cores to simulate three thunderstorms over India. Their results reveal that the NMM core has simulated well the squall line propagation, while in the ARW core the squall line movement was slow. Since the warm WUS LST/SUBT anomaly contributes to SGP extreme precipitation through wave trains propagating eastward, the above suggests that the NMM core has a better advantage to predict such wave trains. Furthermore, Fig. 9a shows that the warm May 2015 WUS LST/SUBT anomaly in Case D3 causes a strong and statistically significant positive vorticity anomaly along with a cyclonic circulation anomaly over the SGP, both of which are due to the aforementioned wave trains propagating eastward. Case C3 exhibits similar features, though with lesser magnitude and extension (Fig. 9b). Another major factor contributing to the occurrence of precipitation is the large-scale vertical motion. Figure 9c, d show the mean vertical velocity (omega) at 850-hPa from Cases D3 and C3, respectively. The negative (positive) values represent rising (sinking) motion. In Case D3 the strong statistically significant negative vorticity anomaly over the SGP yields strong low level convergence, which is in agreement on one hand with the enhancement of moisture transport through the LLJ from the Gulf of Mexico (see Fig. 6e), and on the other hand to the strong rising motion (Fig. 9c) anomaly due to an enhancement in convection. In opposition to Case D3, the strong rising motion anomaly was not properly produced in Case C3 (Fig. 9d). The absence of low-level anomalous negative geopotential height in eastern North America as well as the slight shift of the location of the 500-hPa strong positive geopotential anomaly toward the upper Midwest in early April favor a weakened low level rising motion over the SGP and surrounding areas, where most of the wet precipitation anomaly due to LST/SUBT downstream effects are expected. All of these factors in Case C3 tend to decrease the rainfall amount over the SGP (Fig. 10a), compared to Case D3. However our results also suggest that a weak low-level rising motion alone is not sufficient to inhibit the rainfall anomaly over the SGP when large scale dynamic factors undoubtedly dominate, as through changing of atmospheric moisture transport and vorticity in the upper troposphere can lead to precipitation anomalies. Consequently, Case C3 was able to simulate a positive precipitation anomaly over the SGP, though the anomaly was neither statically significant nor regionally well located (Fig. 10a). Furthermore, we found a consistency between the Case C3 precipitation anomaly in May with low-level wind, vorticity, and vertical motion anomalies, exhibiting particularly dry conditions over the Mid-west and western portion of Texas (Fig. 10a). To further investigate the sensitivity of the LST/SUBT effect on downstream precipitation over North America to the dynamic core, Fig. 10b, c illustrate the area-average precipitation obtained from different cases over the SGP and the CVA (USA as a whole), respectively. Figure 10b shows that over the SGP, though using different domains the simulated precipitation anomalies from the NMM dynamic core range from 0.86 to 1.12 mm/day, while with the ARW dynamic core, the precipitation anomaly does not exceed 0.37 mm/day. These results suggest that, the LST/SUBT effects on downstream precipitation anomaly amounts are more sensitive to the dynamical core than the choice of the domain sizes and highlight the advantage of the NMM core for LST/SUBT downstream effect studies in North America.

Overall, from this analysis it is evident that the choice of dynamical core significantly affects the large scale circulation associated with LST/SUBT effect to downstream precipitation anomaly over North America, along with the SGP rainfall anomaly. The analysis shows that the ARW dynamical core does not simulate dependably the large-scale features, in particular the eastward wave trains along with the strong rising motion over the SGP, which in turn results in an inappropriate simulation of the SGP precipitation anomaly (see Fig. 10b).

3.3 Impact of land surface parameterizations

In this section we explore the sensitivity of the LST/SUBT dynamical downscaling over North America, to surface processes representation within the same model. Cases S3 and Case D3 are generated using the NMM dynamical core, but

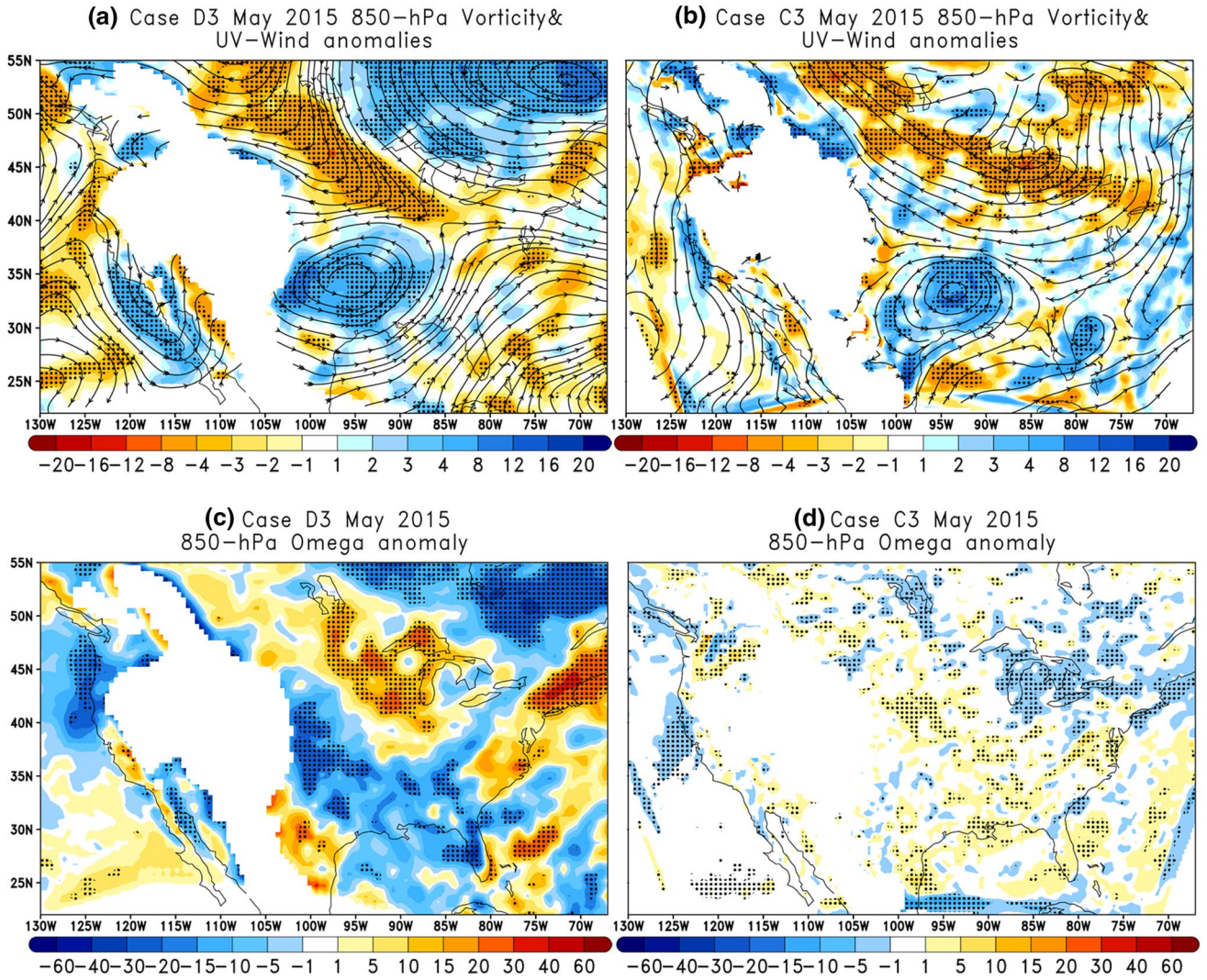

Fig. 9 May 2015 850-hPa vorticity (shaded, unit: m/s) anomaly superimposed with the 850-hPa wind direction (streamlines, unit: m/s) anomaly from: **a** Case D3 and **b** Case C3. May 2015 850-hPa vertical wind (omega; shaded, unit: Pa/s) from: **c** Case D3 and **d** Case C3. The stippled (doted) areas denote regions statistically significant at a 90% confidence level

coupled to different land surface model: SSiB2, and SSiB3, respectively. The main difference of SSiB3 over SSiB2 is the multi-snow layers and the advanced snow-hydrology scheme, which have significant effect on spring snow melting and ground temperature (Sun et al. 1998; Xue et al. 2003). We recall that the same domain, namely domain 3 (D3) is utilized for both Case D3 and Case S3; Fig. 11a-b display the surface temperature anomaly for the first 10 days of integration from Case D3 and Case S3, respectively. The initial imposed warm LST/SUBT anomaly over the WUS produces a warm temperature anomaly, which is visually and numerically comparable during the first 10 days of integration. In weeks 3–4 of April, the warm anomaly over the WUS weakens in both Case D3 and C3. However, with Case D3 being 0.5 °C warmer than Case S3 by the end of April, though the anomaly persisted (not shown). This warm anomaly produced a strong positive geopotential height in the middle troposphere (500-hPa) over the imposed area (Fig. 11c-d). However, in agreement with the difference noticed in the surface warming anomaly, Case D3 produces a stronger positive geopotential height anomaly, which is more centered over the heating region, particularly northwestern United States (from California to south Canada).

The energy and water budget anomalies in May 2015 from Case D3 and Case S3 are summarized in Tables 6 and 7 and shown in Figs. 12 and 13. The warm temperature anomaly in the WUS in Case D3 produces a positive net longwave anomaly over the SGP and along the western half of the US in May 2015. Meanwhile, the net shortwave radiation decreases (Fig. 12a, c), implying an increase in cloud fraction (Fig. 13c). For Case S3, a quite similar pattern is observed but the increase/decrease over SGP is not

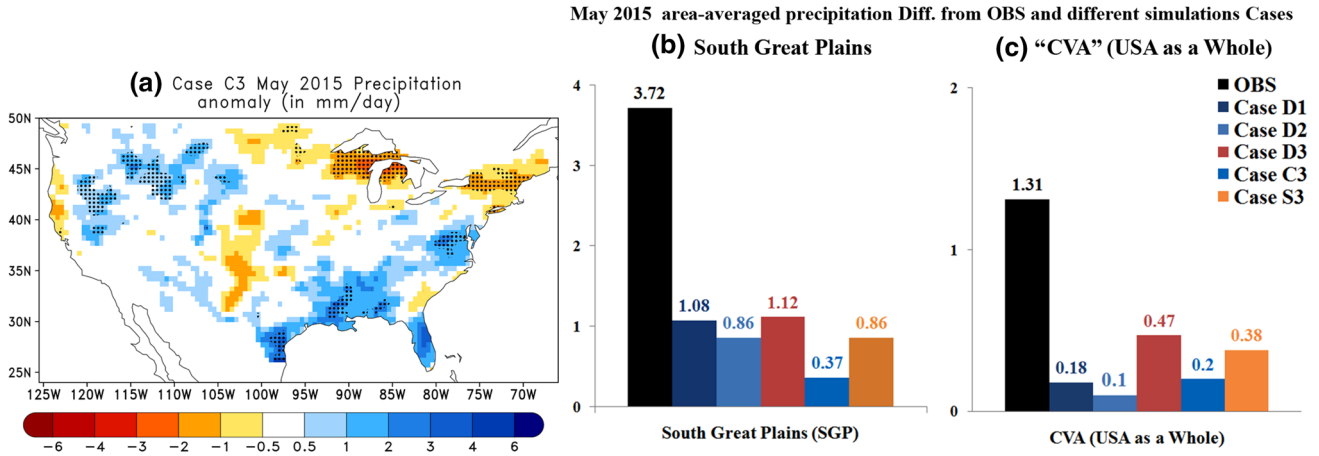

Fig. 10 **a** May 2015 simulated precipitation anomaly (unit: mm/day) over United States from Case C3. **b** Area-average of observed and simulated May 2015 precipitation anomaly (unit: mm/day) over the South Great Plains and adjacent areas (SGP; 105°W–88°W and 29°N–38°N; right) and the whole United States (120°W–80°W and 29°N–49°N, left). The stippled (dots) in **a** indicate areas statistically significant at a 90% confidence level

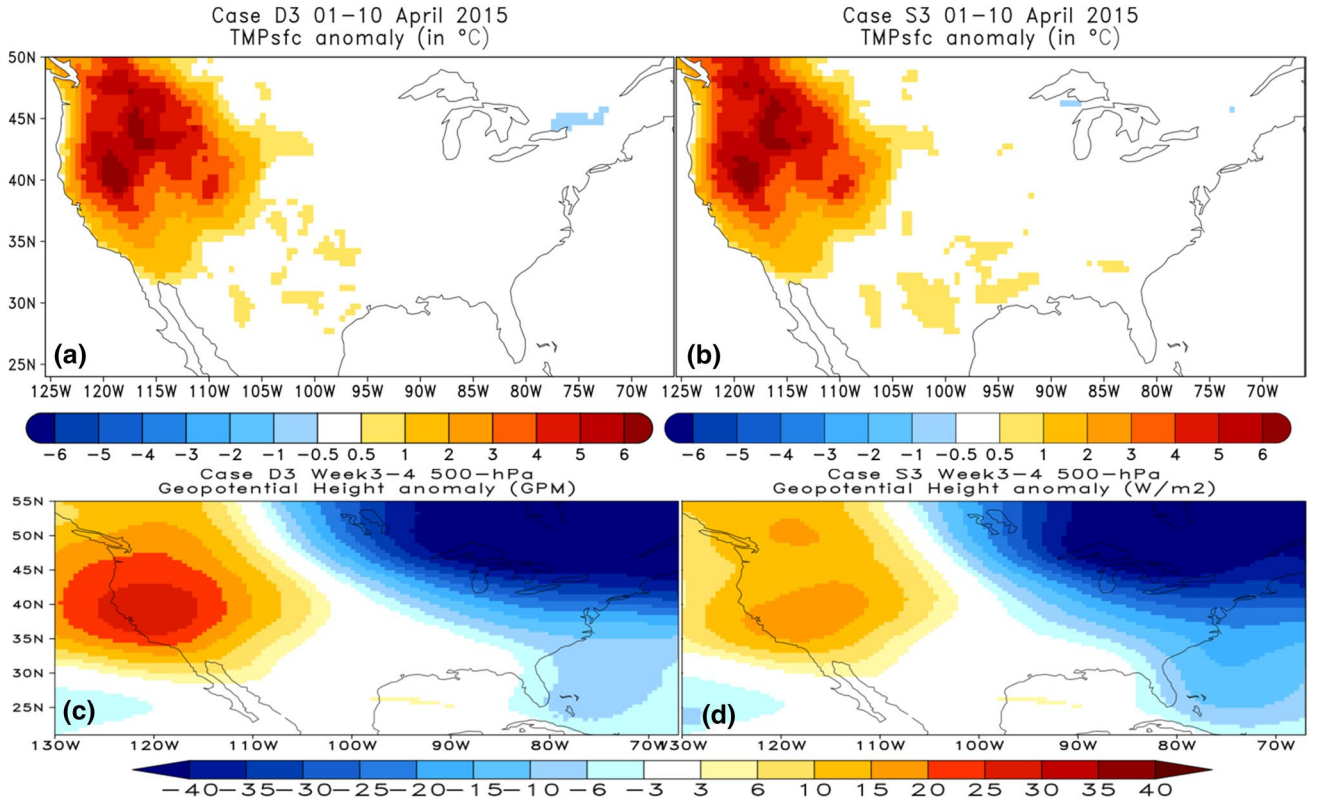

Fig. 11 Simulated surface temperature (unit: °C) differences for the first 10 days from: **a** Case D3 and **b** Case S3. Weeks 3–4 simulated 500-hPa geopotential height (shaded, unit: gpm) anomalies from: **c** Case D3 and **d** Case S3

properly located (Figs. 12b, 13d) because the anomalies tend to be more centered over the border between the Southwest and the northern Great Plains. Over the SGP the Case D3 experiment shows an increase of moisture flux convergence (MFC) associated with an increase in cloud cover, leading to more convective precipitation, which combined with the negative sensible heat flux associated with a cyclonic circulation, contributes to the appropriate simulation of the

Table 6 May 2015 surface energy budget anomaly averaged over Southern Great Plains (88°W–105°W and 29°N–38°N) and Western US (110°W–124.5°W and 35°N–49°N)

Cases	Variables	Southern great plains (SGP)	Western US (WUS)
Case D3	Cloud cover	4.72	6.87
	LHF	− 5.16	− 0.52
	SHF	− 4.96	− 3.60
	Net Rad	− 11.50	− 10.00
	Net LW	8.05	4.20
	Net SW	− 19.54	− 14.20
Case S3	Cloud cover	2.83	5.05
	LHF	− 3.57	1.75
	SHF	− 4.09	− 1.68
	Net Rad	− 7.78	− 7.40
	Net LW	7.26	1.72
	Net SW	− 15.05	− 9.12

Variables are: *LHF* latent heat flux, *SHF* sensible heat flux, *Net Rad* net radiation, *Net LW* net long-wave radiation, and *Net SW* net short-wave radiation; units for fluxes are W m^2 and for Cloud Cover is %

Table 7 May 2015 surface water budget anomaly (Units: mm/day) averaged over the Southern Great Plains (88°W–105°W and 29°N–38°N)

	Precip.	Evap.	MFC.	Conv. Precip.
Case D3	**1.12**	**− 0.19**	**1.32**	**0.95**
Case S3	0.86	− 0.14	1.00	0.86

Variables are: *Precip* precipitation, *Evap* evaporation, *MFC* moisture flux convergence and *Conv. Precip* convective precipitation; units for all variables are mm/day

Highlighted numbers using bold indicate better performance

observed precipitation anomaly (Figs. 12, 13; Tables 6, 7). Case S3 simulates the aforementioned process; however, it fails to properly simulate the regional anomaly.

4 Summary and conclusions

The spring LST and SUBT in the high elevation areas of the Western US have been shown to have significant impacts on downstream summer droughts/floods in North America and East Asia (Xue et al. 2016, 2018). Proper RCM downscaling is crucial for identifying such effects. In this paper, we investigate the sensitivity of the DDM of LST/SUBT downstream effects in North America focusing on the 2015 SGP flood case to: (1) domain size choice and boundary location, (2) change in the dynamical cores within the same regional climate model, and (3) land surface process parameterizations. Results show that all the experiments reproduce the observed surface temperature and precipitation anomalies, particularly the warm temperature anomaly over the WUS, the wet precipitation anomaly over the SGP, and the dry conditions toward the US south eastern region. However, substantial discrepancies regarding the amount of precipitation/surface temperature anomalies and regional anomaly locations occur across the different domains. In fact, along these settings the best simulation of the positive precipitation anomaly over the SGP along with the warm temperature anomaly over the WUS is achieved when the southern boundary is located over the Gulf of Mexico and Caribbean Sea. This finding emphasizes that, although the DDM of the LST/SUBT effect in North America is sensitive to the choice of the domain size, the southern boundary position appears to be more important/crucial. This originates from a more dependable simulation of the strengthening of the SGP LLJ, which in turn brings more moisture from the Gulf of Mexico to the SGP (see Figs. 4, 5, 6, 7).

After identifying an optimum domain size, we utilized that domain size to investigate the effect of change in dynamic cores by comparing the NMM core (Case D3) and the ARW core (Case C3). In North America, the LST/SUBT downstream effects are associated with a large-scale atmospheric stationary wave extending eastward from the LST anomaly region (Xue et al. 2016, 2018). When we compared the results from the two dynamic cores, we found that during the first 10 days of simulation with the ARW dynamic core, the imposed warm anomaly over the WUS produced a positive 500-hPa geopotential height anomaly not located over the 'heated area' (WUS), but rather shifted over the upper Midwest. In addition the eastward propagation of wave trains is not properly simulated, which suppresses the strong rising motion over the SGP. Consequently, the precipitation anomalies could not be properly produced, suggesting that improper simulation of the large-scale features associated with LST/SUBT extreme downstream precipitation led to biases in the amount/location of precipitation anomaly. Thus, the NMM core has performed better in simulating the LST/SUBT downstream effects large-scale features over North America. Additionally, comparison of the SGP precipitation anomaly from the various experiments suggest that the DDM of the LST/SUBT effects on downstream precipitation anomaly amounts are more sensitive to the dynamic core than the domain sizes (see Fig. 10b, c).

We also assessed the sensitivity of LST/SUBT downstream effect to land surface parameterization by intercomparing NMM core simulations over domain 3 using SSiB3 (Case D3; NMM/SSiB3) and SSiB2 (Case S3; NMM/SSiB2) for the representation of vegetation biogeophysical processes. Both Case D3 and Case S3 are able to hold the imposed warm temperature anomaly, however with Case D3 being about 0.5 °C warmer than Case S3 by the end of April. Over the SGP, the Case D3 shows in May 2015 an increase of MFC associated with an increase in cloud cover,

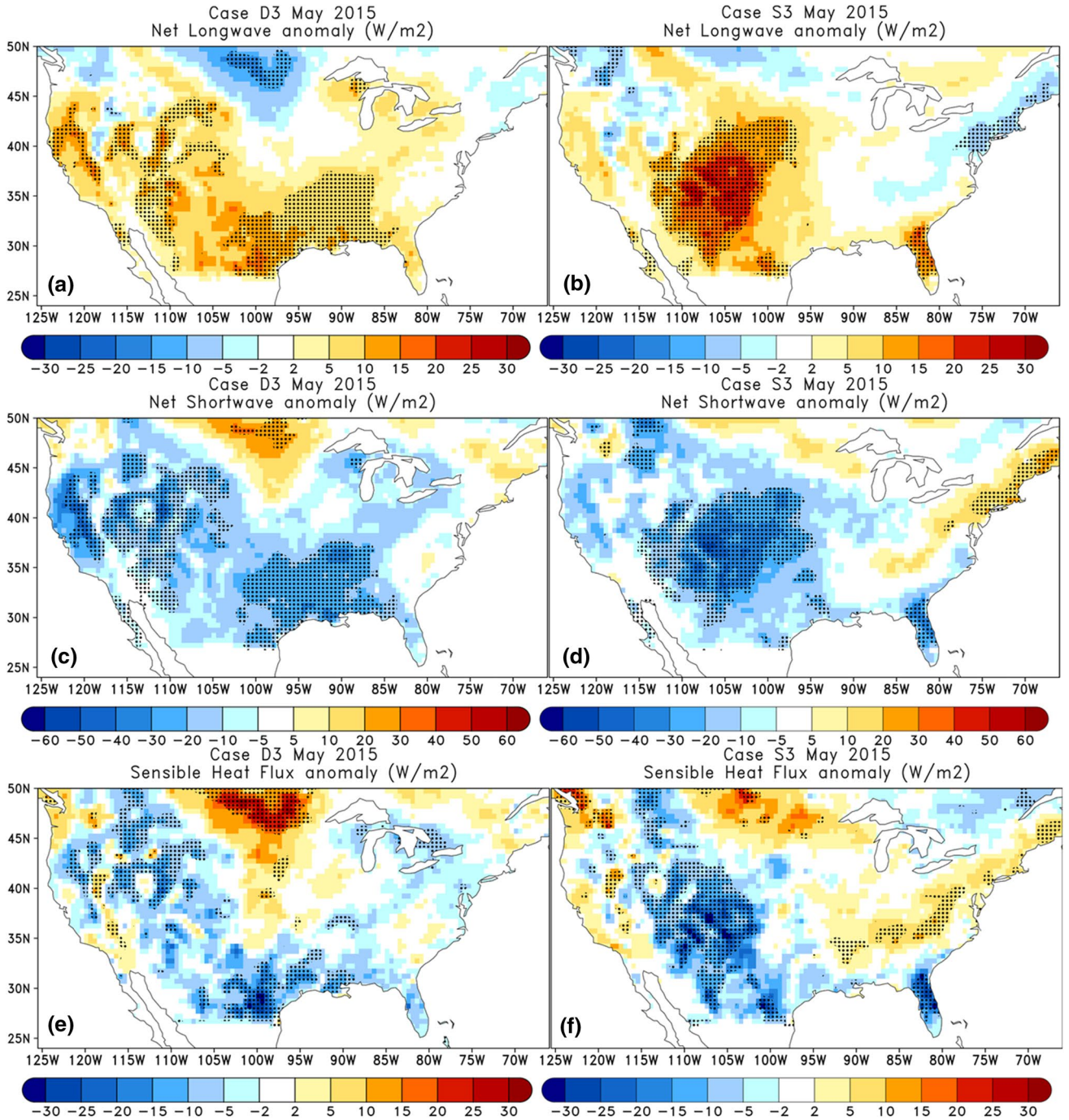

Fig. 12 May 2015 simulated net longwave radiation (top panels, unit: W/m^2), net shortwave radiations (middle panels; units: W/m^2) and surface sensible heat flux (bottom panels; unit: W/m^2) anomalies from: Case D3 (left panels; **a**, **c**, and **e**) and Case S3 (right panels; **b**, **d**, and **f**). The stippled (dotted) areas denote the areas statistically significant at a 90% confidence level

leading to more convective precipitation, which combined together with the negative sensible heat flux associated with a cyclonic circulation, contributed to an appropriate simulation of the observed precipitation anomaly (Figs. 12, 13). Case S3 simulates the aforementioned process; however, it fails to simulate properly the regional anomaly.

In summary, we found at the current stage of the state-of-the-art WRF/SSiB modeling system (NMM/SSiB3, NMM/SSiB2, and ARW/SSiB3) that the LST/SUBT downstream effect is more sensitive to the dynamical core than both the choice of domain size, boundary location and land surface parameterizations. But the effect of spin-up

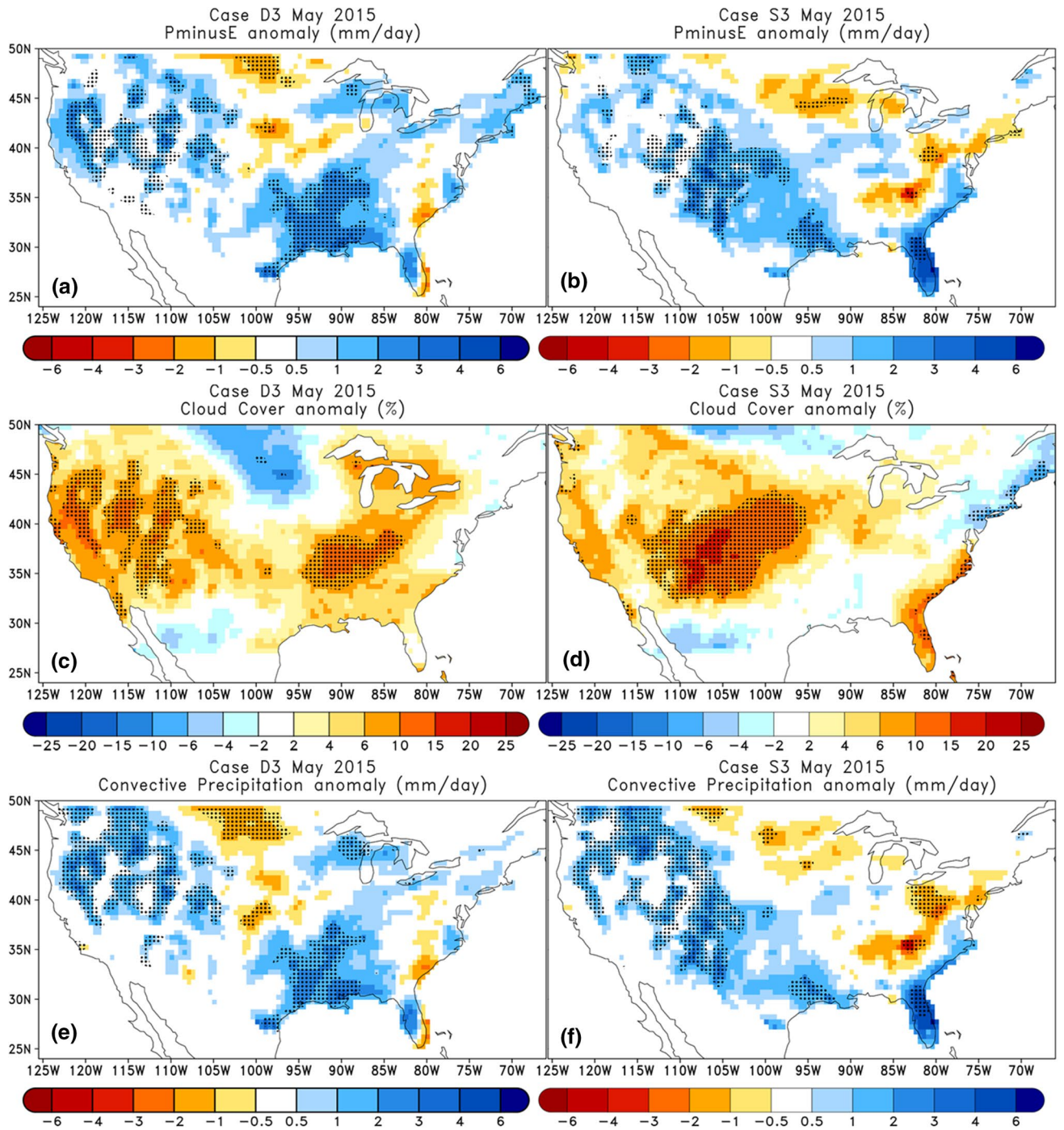

Fig. 13 May 2015 simulated moisture flux convergence (MFC, top panels, unit: mm/day), total cloud cover (middle panels; units: %) and convective precipitation (bottom panels; unit: mm/day) anomalies from: Case D3 (left panels; **a**, **c**, and **e**) and Case S3 (right panels; **b**, **d**, and **f**). The stippled (dotted) areas denote the areas statistically significant at a 90% confidence level

time on the relationship between LST/SUBT anomalies and downstream precipitation anomalies remains an open question, which we leave for future studies. In addition, more studies with more cases using different models over regions having similar geographical settings are needed to test those relationships and general physical principles along with assessing the robustness of our conclusions. The LST/SUBT downstream effects study is still in its early stages and will receive increased attention in the near future (next year's) because recent studies have shown that consideration of LST/SUBT anomalies have the potential

to add value to seasonal/intra-seasonal prediction of downstream extreme hydroclimatic events.

Acknowledgements This study was supported by the following grants from the US National Science Foundation: AGS-1346813 and AGS-1419526. The authors would like to thank NCAR Computational and Information System Laboratory (CISL) for providing invaluable computer time for the model simulations, as well as the three anonymous reviewers' and the editor for providing very constructive comments/suggestions to help improve the quality of the paper. All the model runs described in this study were carried out at the NCAR CISL Yellowstone/Cheyenne high performance cluster (https://doi.org/10.5065/D6RX99HX), sponsored by the National Science Foundation. All simulations datasets analyzed in this study are archived at the Geography Department of University of California, Los Angeles (UCLA) and can be obtained upon request by contacting the corresponding author (idiallo@ucla.edu).

References

Bamba A, Diallo I et al (2018) Effect of the African greenbelt position on West African summer climate: a regional climate modeling study. Theor Appl Climatol. https://doi.org/10.1007/s00704-018-2589-z

Bhaskaran B, Ramachandran A, Jones R, Moufouma-Okia W (2012) Regional climate model applications on sub-regional scales over the Indian monsoon region: the role of domain size on downscaling uncertainty. J Geophys Res. https://doi.org/10.1029/2012JD017956 (**ISSN: 0148–0227**)

Browne NAK, Sylla MB (2012) Regional climate model sensitivity to domain size for the simulation of the West African monsoon rainfall. Int J Geophys. https://doi.org/10.1155/2012/625831

Centella-Artola A, Taylor MA, Bezanilla-Morlot A, Martínez-Castro D, Campbell J, Stephenson T, Vichot-Llano A (2015) Assessing the effect of domain size over the Caribbean region using the PRECIS regional climate model. Clim Dyn 44:1901–1918. https://doi.org/10.1007/s00382-014-2272-8

Chang FC, Wallace JM (1987) Meteorological conditions during heat waves and droughts in the United States Great Plains. Mon Weather Rev 115:1253–1269

Chen M, Shi W, Xie P, Silva VBS, Kousky VE, Wayne Higgins R, Janowiak JE (2008) Assessing objective techniques for gauge based analyses of global daily precipitation. J Geophys Res 113:D04110. https://doi.org/10.1029/2007JD009132

Chen F, Liu C-H, Dudhia J, Chen M (2014) A sensitivity study of high-resolution regional climate simulations to three land surface models over the western United States. J Geophys Res 119:7271–7291. https://doi.org/10.1002/2014JD021827

Cook KH, Vizy EK, Launer ZS, Patricola CM (2008) Springtime intensification of the Great Plains low-level jet and Midwest precipitation in GCM simulations of the twenty-first century. J Clim 21:6321–6340. https://doi.org/10.1175/2008JCLI2355.1

Dash SK, Pattnayak KC, Panda SK, Vaddi D, Mamagain A (2015) Impact of domain size on the simulation of Indian summer monsoon in RegCM4 using mixed convection scheme and driven by HadGEM2. Clim Dyn 44:961–975. https://doi.org/10.1007/s00382-014-2420-1

De Sales F, Xue Y (2011) Assessing the dynamic-downscaling ability over South America using the intensity-scale verification technique. Int J Climatol 31:1205–1221

De Sales F, Xue Y (2013) Dynamic downscaling of 22-year CFS winter seasonal hindcasts with the UCLA-ETA regional climate model over the United States. Clim Dyn 41:255–275

Diallo I, Sylla MB, Giorgi F, Gaye AT, Camara M (2012) Multimodel GCM-RCM ensemble-based projections of temperature and precipitation over West Africa for the Early 21st century. Int J Geophys 2012:1–19. https://doi.org/10.1155/2012/972.896

Diallo I, Bain CL, Gaye AT, Moufouma-Okia W, Niang C, Dieng MDB, Graham R (2014) Simulation of the Wes African monsoon onset using the HadGEM3-RA regional climate model. Clim Dyn 43(3–4):575–594. https://doi.org/10.1007/s00382-014-2219-0

Diallo I, Giorgi F, Sukumaran S, Stordal F, Giuliani G (2015) Evaluation of RegCM4 driven by CAM4 over Southern Africa: mean climatology, interannual variability and daily extremes of wet season temperature and precipitation. Theor Appl Climatol 121(3–4):749–766

Diallo I, Giorgi F, Deme A, Tall M, Mariotti L, Gaye AT (2016) Projected changes of summer monsoon extremes and hydroclimatic regimes over West Africa for the twenty-first century. Clim Dyn 47(12):3931–3954. https://doi.org/10.1007/s00382-016-3052-4

Diallo I, Giorgi F, Stordal F (2018) Influence of Lake Malawi on regional climate from a double-nested regional climate model experiment. Clim Dyn 50(9–10):3397–3411. https://doi.org/10.1007/sOO382-017-3811-x

Dodla VB, Desamsetti S, Yerramilli A (2011) A comparison of HWRF, ARW and NMM models in Hurricane Katrina (2005) simulation. Int J Environ Res Public Health 8:2447–2469

Dong X, Baike X, Kennedy A, Feng Z, Entin JK, Houser PR, Schiffer RA, L'Ecuyer T, Solson WS, Hsu K, Liu WT, Lin B, Deng Y, Jiang T (2011) Investigation of the 2006 drought and 2007 flood extremes at the Southern Great Plains through an integrative analysis of observations. J Geophys Res Atmos 116(D03204). https://doi.org/10.1029/2010JD014776

Fan Y, van den Dool H (2008) A global monthly land surface air temperature analysis for 1948-present. J Geophys Res. https://doi.org/10.1029/2007JD008470

Fels SB, Schwarzkopf MD (1981) An efficient, accurate algorithm for calculating CO2 15 μm band cooling rates. J Geophys Res 86:1205–1232

Ferrier B (1994) A double-moment multiple-phase four-class bulk ice scheme. Part 1: description. J Atmos Sci 51:249–280

Fotso-Nguemo TC, Vondou DA, Pokam WM, Djomou ZY, Diallo I, Haensler A, Tchotchou LA, Kamsu-Tamo PH, Gaye AT, Tchawoua C (2017) On the added value of the regional climate model REMO in the assessment of climate change signal over Central Africa. Clim Dyn 49(11–12):3813–3838. https://doi.org/10.1007/s00382-017-3547-7

Gallus WA, Bresch JF (2006) Comparison of impacts of WRF dynamic core, physics package, and initial conditions on warm season rainfall forecasts. Mon Weather Rev 134(9):2632–2641

Gao XJ, Shi Y, Zhang DF et al (2012) Uncertainties of monsoon precipitation projection over China: results from two high resolution RCM simulations. Clim Res 52:213–226

Giorgi F, Gutowsky WJ (2016) Coordinated experiments for projections of regional climate change. Curr Clim Change Rep 2:202–210

Giorgi F, Mearns LO (1999) Introduction to special section: regional climate modelling revisited. J Geophys Res 104:6335–6352

Grell GA, Devenyi D (2002) A generalized approach to parameterizing convection combining ensemble and data assimilation techniques. Geophys Res Lett 29(14):38-1–38-4. https://doi.org/10.1029/2002gl015311

Gu Y, Liou KN, Ou SC, Fovell R (2011) Cirrus cloud simulations using WRF with improved radiation parameterization and increased vertical resolution. J Geophys Res. https://doi.org/10.1029/2010jd014574

Harding KJ, Snyder PK (2015) The relationship between the Pacific–North American teleconnection pattern, the Great Plains

low-level jet, and North Central us heavy rainfall events. J Clim. https://doi.org/10.1175/JCLI-D-14-00657.1
Hoerling M, Eischeid J, Kumar A, Leung R, Mariotti A, Mo K, Schubert S, Seager R (2014) Causes and predictability of the 2012 Great Plains drought. Bull Am Meteorol Soc 95(2):269–282
Hong SY, Pan HL (1996) Non-local boundary layer vertical diffusion in a medium range forecast model. Mon Weather Rev 124:2322–2339
Hong SY, Pan HL (1998) Convective trigger function for a mass-flux cumulus parameterization scheme. Mon Weather Rev 126:2599–2620
Hong SY, Noh Y, Dudhia J (2006) A new vertical diffusion package with an explicit treatment of entrainment processes. Mon Weather Rev 134(9):2318–2341
Hou YT, Moorthi S, Campana KA (2002) Parameterization of solar radiation transfer in the NCEP models. NCEP Office Note, p 441. http://www.emc.ncep.noaa.gov/officenotes/FullTOC.html#2000
Hu X-M, Xue M, McPherson RA, Martin E, Rosendahl DH, Qiao L (2018) Precipitation dynamical downscaling over the Great Plains. J Adv Model Earth Syst 10:421–447. https://doi.org/10.1002/2017MS001154
Janjic ZI (2001) Nonsingular implementation of the Mellor–Yamada level 2.5 scheme in the NCEP Meso Model. NCEP Office Note 437:61
Janjic Z, Gerrity J, Nickovic S (2001) An alternative approach to nonhydrostatic modeling. Mon Weather Rev 129:1164–1178
Jee J, Kim S (2017) Sensitivity study on high-resolution WRF precipitation forecast for a heavy rainfall event. Atmosphere 2017(8):96. https://doi.org/10.3390/atmos8060096
Kanamitsu M, Ebisuzaki W, Woollen J, Yang S-K, Hnilo JJ, Fiorino M, Potter GL (2002) NCEP-DOE AMIP-II Reanalysis (R-2). Bull Am Meteor Soc 83:1631–1643
Koster RD, Chang Y, Wang H, Schubert SD (2016) Impacts of local soil moisture anomalies on the atmospheric circulation and on remote surface meteorological fields during boreal summer, a comprehensive analysis over North America. J Clim 29:7345–7364
Koster RD, Betts AK, Dirmeyer PA, Bierkens M, Bennett KE et al (2017) Hydroclimatic variability and predictability: a survey of recent research Hydrol. Earth Syst Sci 21:3777–3798
Leduc M, Laprise R (2009) Regional climate model sensitivity to domain size. Clim Dyn 32:833–854. https://doi.org/10.1007/s00382-008-0400-z
Lee J, Xue Y, De Sales F et al (2018) Evaluation of multi-decadal UCLA-CFSv2 simulation and impact of interactive atmospheric-ocean feedback on global and regional variability. Clim Dyn. https://doi.org/10.1007/s00382-018-4351-8
Li W, Guo W, Xue Y, Fu C, Qiu B (2016) Sensitivity of a regional climate model to land surface parameterization schemes for East Asian summer monsoon simulation. Clim Dyn 47(7–8):2293–2308. https://doi.org/10.1007/s00382-015-2964-8
Litta AJ, Idicula SM, Mohanty UC, Prasad SK (2012) Comparison of thunderstorm simulations from WRF-NMM and WRF-ARW models over East Indian Region. Sci World J. https://doi.org/10.1100/2012/951870
Mariotti L, Diallo I, Coppola E, Giorgi F (2014) Seasonal and intraseasonal changes of African monsoon climates in 21st century CORDEX projections. Clim Change. https://doi.org/10.1007/s10584-014-1097-0
Mearns LO, Arritt R, Biner S, Bukovsky MS, McGinnis S, Sain S, Caya D, Correia J, Flory D, Gutowski W, Takle ES, Jones R, Leung R, Moufouma-Okia W, McDaniel L, Nunes AMB, Qian Y, Roads J, Sloan L, Snyder M (2012) The north American regional climate change assessment program overview of phase I results. Bull Am Meteorol Soc 93:1337–1362
Mei R, Wang G (2012) Summer land-atmosphere coupling strength in the United States: comparison among observations, reanalysis data, and numerical models. J Hydrometeorol 13:1010–1022
Mekonnen A, Renwick JA, Sánchez-Lugo A (eds) (2016) Regional climates [in "State of the Climate in 2015"]. Bull Am Meteorol Soc 97(8):S173–S226
Mesinger F, DiMego G, Kalnay E, Mitchell K, Shafran PC, Ebisuzaki W, Jovic D, Woollen J, Rogers E, Berbery EH, Ek MB, Fan Y, Grumbine R, Higgins W, Li H, Lin Y, Manikin G, Parrish D, Shi S (2006) North American regional reanalysis. Bull Am Meteorol Soc 87:343–360
Moorthi S, Pan HL, Caplan P (2001) Changes to the 2001 NCEP operational MRF/AVN global analysis/forecast system. NWS Tech Proced Bull 484:1–14. http://www.nws.noaa.gov/om/tpb/484.htm
Oaida CM, Xue Y, Flanner MG, Skiles SM, De Sales F, Painter TH (2015) Improving snow albedo processes in WRF/SSiB regional climate model to assess impact of dust and black carbon in snow on surface energy balance and hydrology over western US. J Geophys Res 120:3228–3248. https://doi.org/10.1002/2014jd022444
Patricola CM, Chang P, Saravanan R (2015) Impact of Atlantic SST and high frequency atmospheric variability on the 1993 and 2008 Midwest floods: regional climate model simulations of extreme climate events. Clim Change 129:397–411
Poan ED, Gachon P, Laprise R, Aider R, Dueymes G (2018) Investigating added value of regional climate modeling in North America winter storm track simulations. Clim Dyn 50:1799–1818. https://doi.org/10.1007/s00382-017-3723-9
Pu B, Fu R, Dickinson RE, Fernando DN (2016) Why do summer droughts in the Southern Great Plains occur in some La Niña years but not others? J Geophys Res Atmos 121. https://doi.org/10.1002/2015JD023508
Rummukainen M (2010) State-of-the-art with regional climate models. WIRE Adv Rev 1(1):82–96
Ryu J-H, Hayhoe K (2017) Observed and CMIP5 modeled influence of large-scale circulation on summer precipitation and drought in the South-Central United States. Clim Dyn 49(11–12):4293–4310. https://doi.org/10.1007/s00382-017-3534-z
Saini R, Wang G, Pal JS (2016) Role of soil moisture feedback in the development of extreme summer drought and flood in the United States. J Hydrometeorol 17(8):2191–2207
Seth A, Giorgi F (1998) The effects of domain choice on summer precipitation simulation and sensitivity in a regional climate model. J Clim 11(10):2698–2712
Seager R, Neelin D, Simpson I, Liu H, Henderson N, Shaw T, Kushnir Y, Ting M, Cook B (2014) Dynamical and thermodynamical causes of large-scale changes in the hydrological cycle over North America in response to global warming. J Clim 27:7921–7948. https://doi.org/10.1175/JCLI-D-14-00153.1
Skamarock WC, Klemp JB, Dudhia J, Gill DO, Barker DM, Duda MG, Huang X-Y, Wang W, Powers JG (2008) A description of the advanced research WRF version 3. NCAR technical note, NCAR/TN-475+STR, National Center for Atmospheric Research, Boulder
Song IS, Byun U-Y, Hong J, Park SH (2018) Domain-size and top-height dependence in regional predictions for the Northeast Asia in spring. Atmos Sci Lett. https://doi.org/10.1002/asl.799
Sun S, Xue Y (2001) Implementing a new snow scheme in simplified simple biosphere model. Adv Atmos Sci 18:335–354. https://doi.org/10.1007/BF02919314
Sun S, Jin J, Xue Y (1998) A simple snow-atmosphere-soil transfer model. J Geophys Res Atmos 104:19587–19597
Sun X, Xue M, Brotzge J, McPherson R, Hu X-M XQ, Yang XQ (2016) An evaluation of dynamical downscaling of central plains summer precipitation using a WRF-based regional climate model at a convection-permitting 4 km resolution. J Geophys Res Atmos 121:13801–13825. https://doi.org/10.1002/2016JD024796

Torma C, Giorgi F, Coppola E (2015) Added value of regional climate modeling over areas characterized by complex terrain—precipitation over the Alps. J Geophys Res Atmos 120:3957–3972

Van Den Broeke MS, Kalin A, Alavez JAT, Oblesby R, Hu Q (2017) A warm-season comparison of WRF coupled to the CLM4.0, Noah-MP, and Bucket hydrology land surface schemes over the central USA. Theor Appl Climatol. https://doi.org/10.1007/s00704-017-2301-8

Vannitsem SF, Chomé F (2005) One-way nested regional climate simulations and domain size. J Clim 18:229–233

Vidale PL, Luthi C, Frei D, Seneviratne S, Schar C (2003) Predictability and uncertainty in a regional climate model. J Geophys Res Atmos 108(D18):4586 do

Wang S-Y, Huang W-R, Hsu H-H, Gillies RR (2015) Role of the strengthened El Niño teleconnection in the May 2015 floods over the southern Great Plains. Geophys Res Lett 42:8140–8146

Weaver SJ, Schubert S, Wang H (2009) Warm season variations in the low-level circulation and precipitation over the central United States in observations, AMIP simulations, and idealized SST experiment. J Clim 22:5401–5420

Xue Y, Sellers PJ, Kinter JL, Shukla J (1991) A simplified biosphere model for global climate studies. J Clim 4(3):345–364

Xue Y, Fennessy MJ, Sellers PJ (1996) Impact of vegetation properties on US summer weather prediction. J Geophys Res 101:7419–7430

Xue Y, Zeng FJ, Mitchell KE, Janjic Z, Rogers E (2001) The impact of land surface processes on simulations of the US Hydrological cycle: a case study of the 1993 flood using the SSiB land surface model in the NCEP eta regional model. Mon Weather Rev 129:2833–2860

Xue Y, Sun S, Kahan DS, Jiao Y (2003) Impact of parameterizations in snow physics and interface processes on the simulation of snow cover and runoff at several cold region sites. J Geophys Res 108(D22):8859. https://doi.org/10.1029/2002JD003174

Xue Y, Juang HM, Li W, Prince S, DeFries R, Jiao Y, Vasic R (2004) Role of land surface processes in monsoon development: East Asia and West Africa. J Geophys Res 109:D03105. https://doi.org/10.1029/2003JD003556

Xue Y, Vasic R, Janjic Z, Mesinger F, Mitchell KE (2007) Assessment of dynamic downscaling of the continental US regional climate using the Eta/SSiB regional climate model. J Clim 20:4172–4193. https://doi.org/10.1175/jcli4239.1

Xue Y, De Sales F, Vasic R, Mechoso CR, Prince SD, Arakawa A (2010) Global and temporal characteristics of seasonal climate/vegetation biophysical process (VBP) interactions. J Clim 23:1411–1433

Xue Y, Vasic R, Janjic Z, Liu YM, Chu PC (2012) The impact of spring subsurface soil temperature anomaly in the western US on North American summer precipitation: a case study using regional climate model downscaling. J Geophys Res Atmos 117(D11):D11103

Xue Y, Janjic Z, Dudhia J, Vasic R, De Sales F (2014) A review on regional dynamical downscaling in intraseasonal to seasonal simulation/prediction and major factors that affect downscaling ability. Atmos Res 147–148:68–85. https://doi.org/10.1016/j.atmosres.2014.05.001

Xue Y, Oaida CM, Diallo I, Neelin JD, Li S, De Sales F, Gu Y, Robinson D, Vasic R, Yi L (2016) Spring land temperature anomalies in northwestern US and the summer drought over Southern Plains and adjacent areas. Environ Res Lett 11:044018. https://doi.org/10.1088/1748-9326/11/4/044018

Xue Y, Diallo I, Li W, Neelin JD, Chu P-C, Vasic R, Guo W, Li Q, Robinson DA, Zhu Y, Fu C, Oaida CM (2018) Spring land surface and subsurface temperature anomalies and subsequent downstream late spring-summer droughts/floods in North America and East Asia. J Geophys Res Atmos. https://doi.org/10.1029/2017JD028246

Zhan XW, Xue YK, Collatz GJ (2003) An analytical approach for estimating CO2 and heat fluxes over the Amazonian region. Ecol Model 162:97–117

Zhao Q, Carr FH (1997) A prognostic cloud scheme for operational NWP models. Mon Weather Rev 125:1931–1953

Publisher's Note Springer Nature remains neutral with regard to jurisdictional claims in published maps and institutional affiliations.